www.sciencemag.org/content/353/6307/1549/suppl/DC1

Supplementary Materials for

Cyclin A2 is an RNA binding protein that controls *Mre11* mRNA translation

Arun Kanakkanthara, Karthik B. Jeganathan, Jazeel F. Limzerwala, Darren J. Baker, Masakazu Hamada, Hyun-Ja Nam, Willemijn H. van Deursen, Naomi Hamada, Ryan M. Naylor, Nicole A. Becker, Brian A. Davies, Janine H. van Ree, Georges Mer, Virginia S. Shapiro, L. James Maher III, David J. Katzmann, Jan M. van Deursen*

*Corresponding author. Email: vandeursen.jan@mayo.edu

Published 30 September 2016, *Science* **353**, 1549 (2016)
DOI: 10.1126/science.aaf7463

This PDF file includes:

Other supplementary material for this manuscript includes the following:

Tables S1 to S3 (Excel format)

Materials and Methods

Generation of mouse mutants and tumor analysis

The hypomorphic *Ccna2* allele (H), was generated using a gene targeting approach as described previously (*17*). Briefly, targeted ES cell clones were injected into blastocysts, and $Ccna2^{+/H}$ offspring were obtained from the resulting chimeras through standard procedures. The $Ccna2^{-}$ allele was from gene trapped mouse embryonic stem (ES) cell clone DC0194 (Bay Genomics). All animals were maintained on a 129/Sv × C57BL/6 genetic background. DMBA tumor bioassays were performed as previously described (*18*). The DMBA-treated animals were sacrificed at 5 months of age, and screened for lung and skin tumors. Mice in spontaneous tumor susceptibility study were sacrificed at 16 months, and their major organs were screened for overt tumors. Tumors were processed for histopathology by standard procedures.

Mice with deletions in Mre11 3' UTR ($Mre11^{\Delta A2}$) were generated using a pair of single-guide RNAs (sgRNAs) co-injected with WT Cas9 mRNA (L-6125, TriLink Biotechnologies) into the cytoplasm of FVB strain (Envigo) zygotes. The sgRNAs were selected using the WTSI Genome Editing Tool (*19*). We cloned the oligos for the sgRNAs into the pX330U6-Chimeric_ BB-CBh-hSpCas9 vector and used PCR to amplify the sgRNA template and add T7 promoter sequence (*20*). The pX330-U6-Chimeric_BB-CBh-hSpCas9 was a gift from Feng Zhang (Addgene plasmid # 42230) (*21*). The PCR product was purified by QIAquick Gel Extraction Kit and then by QIAquick PCR Purification Kit (Qiagen) following manufacture's instructions. We prepared sgRNAs using the MEGAshortscript T7 Transcription Kit (Thermo Fischer Scientific) and purified PCR products as templates. sgRNAs were purified using the MEGAclear Kit (Thermo Fischer Scientific) according to the manufacture's instructions. The injections were performed with 100 ng/µl Cas9 mRNA and 50 ng/µl of each sgRNA in water. The founder animals were screened by PCR with primers flanking the sgRNA targeting sites followed by subcloning of the PCR products and sequencing. All the primers used are listed in the Table S4. All mouse experiments were conducted after approval of the Mayo Clinic Institutional Animal Care and Use Committee. All mice were housed in a pathogen-free barrier environment.

Cell culture

Primary $Ccna2^{+/+}$ and $Ccna2^{-/H}$ MEFs were generated from E13.5 embryos by standard procedures (*18*). MEFs were frozen at passage 2 (P2) or 3 and used for experimentation between P4 and P6. Mitotic MEFs were prepared by culturing asynchronous cells for 5 h in medium containing 100 ng/ml nocodazole (Sigma-Aldrich) and harvesting cells by shake off. At least three independently generated MEF lines per genotype were used. Procedures for synchronization of MEFs were as previously detailed (*22*). MEF, HEK 293T, HeLa, and human fibroblasts were cultured in DMEM (GIBCO BRL) supplemented with 10% heat-inactivated fetal bovine serum (FBS) and 1% antibiotic/antimycotic solution (GIBCO BRL).

Generation of expression constructs

Lentiviral expression vectors for the full-length human *CCNA1* (Origene #MR225092), *CCNA2* and human *MRE11* were generated by subcloning the coding sequences into the

pTSiN-puro lentiviral vector (*23*). The full-length cDNA clone of *CCNA2* was used as a template for PCR to create cDNAs coding for cyclin A2 (1-301) and cyclin A2 (302-432) proteins. Each construct, except *MRE11*, was provided with an amino-terminal hemagglutinin (HA) epitope tag. Virus production was performed as previously described (*24*). The day before infection, P2 MEFs were seeded at $1x10^6$ cells per T75 culture flask, and infected with freshly harvested lentiviral supernatants every 24 h for 2 infection cycles. Virally transduced MEFs were selected in 2 μg/ml puromycin for 48 h before being used in experiments.

Karyotype analysis

Metaphase spreads of MEFs and splenocytes were prepared and analyzed for numerical and structural chromosomal abnormalities as previously described (*18*).

Knockdown experiments

Knockdown was achieved by using shRNA clones NM_001237.3-1448s21C1 and NM_001237.3-2013s21C1 for cyclin A2; NM_018736.2-602s1C1 and NM_018736.2-2501s1C1 for Mre11; NM_009012.1-2146s1C1 and NM_009012.1-4021s1C1 for Rad50. Non-targeting shRNA TRC1 or 2 was used as a negative control vector.

Live cell imaging

For chromosome missegregation analysis, P2 primary MEFs were first transduced with a lentivirus expressing an mRFP-tagged H2B. Cells were then seeded onto 35-mm glass-bottomed culture dishes (MatTek Corp.). Approximately 24 h later, the chromosome movements of H2B-mRFP positive MEFs progressing through an unchallenged mitosis were followed at interframe intervals of 2 min as previously described (*25*). The experiments were performed using a microscope system (Axio Observer; Zeiss) with CO_2 Module S, TempModule S, Heating Unit XL S, a Plan Apo ×63 NA 1.4 oil differential interference contrast III objective (Zeiss), camera (AxioCam MRm; Zeiss) and AxioVision 4.6 software (Zeiss). Imaging medium was kept at 37°C. Nocodazole challenge assay was performed as previously described (*23*). The separase biosensor experiment was performed and quantified as previously described (*12*), except cells were monitored at 2 min intervals rather than 3 min intervals. At least three independent MEF lines per genotype were used in all the experiments. For assessment of the relationship between spindle geometry and chromosome lagging in *Ccna2*$^{-/H}$ MEFs by live-cell imaging we visualized chromosomes with H2B-YFP and centrosomes with γ-tubulin-tdTomato. Lentivirus expressing H2B-YFP was generated as described (*25*). γ-tubulin-tdTomato fusion protein-expressing lentivirus was generated by PCR based cloning methods using the following oligonucleotide primers: forward primer -γ-tubulin, 5'-TTTTGCTAGCGCCACCATGCCGAGAGAAAT CATCACCCTACA-3'; reverse primer for -γ-tubulin 5'-TTTTACCGGTCTGCTCCT GGGTGCCCCA-3'; forward primer for tdTomato 5'-TTTTACCGGTATGGTGAGCA AGGGCGAGGAGGTC-3' reverse primer for td-Tomato 5'-TTTTGAATTCTTACTTG TACAGCTCGTCCATGCCG-TACA-3'. TdTomato and γ-tubulin PCR products were then cloned into the Xba1 and EcoR1 sites of the pLenti-UbC vector to generate a γ-tubulin-tdTomato fusion protein. *Ccna2*$^{-/H}$ MEFs expressing H2B-YFP and γ-tubulin-tdTomato were monitored as they

progressed through an unchallenged mitosis as described above. To determine the spindle angle of the cells at metaphase, we used the "angle disconnected" tool of ZEN software. The angle formed by the intersection of the line connecting the centers of 2 centrosomes as well as the line passing through the middle of the metaphase plate was used for measurements. Spindles were considered symmetric if the spindle angle was between 85^{o}-95^{o} and asymmetric if they were $<85^{o}$ or $>95^{o}$. Cells in still frames at metaphase, just prior to anaphase onset, were used for angle measurements.

GFP-α-tubulin photoactivation and analysis

MEFs transduced with photoactivatable GFP-α tubulin lentivirus were grown in 35-mm glass-bottomed culture dishes for 24 h, then photoactivated and fluorescence dissipation after photoactivation was analyzed as previously described (*12*).

Cell cycle analysis

For the cell cycle analysis by propidium iodide, cells were harvested and fixed in 95% ethanol for 5 min on ice. Cells were washed and treated with RNase before being stained with propidium iodide (100 μg/ml in 1% sodium citrate). After 15 min incubation in the dark, cell cycle profiles were analyzed by flow cytometry. Additionally, FUCCI analysis of cell cycle profiles of *Ccna2*$^{+/+}$ and *Ccna2*$^{-/H}$ MEFs was carried out as previously described (*12*).

Immunostaining and confocal microscopy analysis

For cyclin A2/γ-tubulin and p-CDK substrate/γ-tubulin staining, cells were fixed in PBS/3% paraformaldehyde (PFA) for 12 min at room temperature (RT), permeabilized in PBS/0.2% Triton X-100 for 10 min and blocked in PBS/1% BSA for 30 min at RT. For γ-tubulin/α-tubulin and Eg5/α-tubulin staining, cells were fixed in PBS/1% PFA for 5 min at RT and then fixed in ice-cold methanol for 10 min at RT. For spindle geometry analysis, serial optical sections were collected from γ-tubulin/α-tubulin stained MEFs using a laser-scanning microscope. After maximum intensity projection, ZEN software (Zeiss) was used to measure the angle between the spindle and the metaphase plate. Cells that had an acute angle between the spindle pole axis and the metaphase plate of less than 85° or greater than 95° were considered asymmetrical. For centrosome distance measurements in G2 and prophase, cells were stained for pH3^{S10}/γ-tubulin/Hoechst, and images were taken by laser-scanning microscopy of cells with centrosomes in the same focal plane. The distance between centrosomes (γ-tubulin signals) was measured using ZEN software (Zeiss). G2 cells with centrosome distances ≥ 3 μm were classified as accelerated. Prophases with centrosome distance/nuclear diameter ratio ≤ 0.5 were considered delayed. For γ-H2Ax/53BP1, γ-H2Ax/Rad51, Mre11/ pH3^{S10} staining, cells were fixed in PBS/3% PFA for 12 min at RT. For Rad50/γ-tubulin staining, cells were fixed in PBS/3% PFA for 12 RT, permeabilized in PBS/0.2% Triton X-100 for 10 min. For γ–H2Ax/RPA-2 staining, cells were fixed in PBS/1% PFA for 1 min, permeabilized in PBS/0.5% Triton X-100 for 5 min and fixed in PBS/3% PFA for 15 at RT. Topo IIα and ACA staining was performed as described previously (*26*). Quantification of cyclin A2, p-CDK substrates, Eg5, Mre11, and Rad50 signals was carried out using ImageJ software (NIH). Confocal microscopy images were converted to eight-bit grey scale, and the mean pixel intensity

density (arbitrary units) within the marked area was calculated. All confocal images are representative of at least three independent experiments.

Primary antibodies for immunostaining were as follows: rabbit cyclin A2 (1:10,000) (*27*); rabbit anti-p-Cdk substrates (1:1,000, 9447, Cell Signaling Technology); mouse anti-phospho-histone H2AX (1:500, 05-636, Millipore); rabbit anti-53BP1 (1:500, NB100-305, Novus Biologicals); rabbit anti-Topo IIα (1:300, TG2011-1, Topogen); human anti-centromeric antibody (1:100, 15-234-0001, Antibodies, Inc.); rabbit anti-Eg5 (1:100, TA301478, Origene); mouse or rabbit anti γ-tubulin (1:300, T6557/clone GTU-88 or T5192, Sigma); mouse anti-α-tubulin (1:1000, T9026/clone DM1A, Sigma); rabbit anti-$pH3^{S10}$ (1:10,000, 06-570, Millipore); rabbit RPA-2 (1:200, ab61184, Abcam); mouse Mre11 (1:500, SC-135992, Santa Cruz), rabbit Rad50 (1:500, ab124682, Abcam), rabbit Rad51 (1:500, GTX100469, GeneTex).

DNA fiber assays

Approximately 2.5 x 10^5 cells were plated in each well of a six-well plate and cultured for 2 days at 37°C in a 5% CO_2 incubator. Cells were pulse-labeled with 50 μM CIdU (C6891, Sigma) for 30 min, washed with pre-warmed (37°C) PBS, and pulsed with 250 μM IdU (I7125, Sigma) for 30 min. The cells were harvested and resuspended in 500 μl of ice-cold PBS. Cell suspension (8 μl) was spotted on one side of a glass slide, and mixed gently with 15 μl of fiber lysis solution (200 mM Tris-HCl, pH 7.4, 50 mM EDTA, and 0.5% SDS). After 8 min incubation at RT, the slide was inclined at 45° to allow the fibers spread along the glass slide. Once dried, DNA spreads were fixed with methanol-acetic acid (3:1) for 10 min. The slides were washed 3 times in PBS, and the DNA was denatured with 2M HCl for 80 min. After washing with PBS, the slides were blocked with 5% BSA in PBS for 30 min and incubated with the following antibodies: rat anti-BrdU monoclonal antibody (for CldU) (1:1000, clone BU1/75 (ICR1), Serotec), and mouse anti-BrdU monoclonal antibody (for IdU) (1:25, clone B44, Becton Dickinson). After incubation in a humid chamber overnight, slides were washed three times, and incubated with AlexaFluor 488-conjugated goat anti-rat and AlexaFluor 594-conjugated goat anti-mouse immunoglobulin G (IgG) (Molecular Probes) secondary antibodies. The images are representative of 3 lines for each genotype.

Western blotting and antibodies

Western blot analysis was carried out as described before (*23*). Tissue lysates were prepared by grinding snap-frozen tissues into powder, then suspending 10 mg of the powder in 100 μl PBS and 100 μl 2x Laemmli lysis buffer, and boiling for 10 min. Whole-cell extracts of MEFs, human fibroblasts, 293T, and HeLa cells were prepared by suspending the cell pellets in PBS (10 μl PBS/10,000 cells) and equal volume of 2× Laemmli lysis buffer, and boiling for 10 min. Primary antibodies for western blotting were as follows: rabbit anti-cyclin A2 (1:80,000)(*27*); mouse anti-cyclin A2 (1:10,000, E23.1, Abcam); mouse anti-actin (1:10,000, A5441/clone AC-15, Sigma-Aldrich); rabbit anti-cyclin A1 (1:1000, ab133183, Abcam); mouse anti-HA (1:1,000, 12013819001/clone 3F10, Roche); rabbit anti-$pH3^{S10}$ (1:10,000, 06-570, Millipore); mouse Mre11 (1:100, SC-135992, Santa Cruz); rabbit Rad50 (1:500, ab124682, Abcam); rabbit anti-Eg5 (1:100, TA301478, ORIGENE); rabbit anti-$pEg5^{T927}$ (1:1000, 620502, BioLegend), rabbit anti-eIF4A2 (1:1000,

ab31218, Abcam); mouse anti-Cdk2 (1:1000, D-12, sc6248); mouse anti-Cdk1 (1:1000, 610038, BD Biosciences); rabbit anti-cyclin E1 (1:5000, ab71535, Abcam); rabbit cyclin B1 (1:1000, 4138S, Cell Signaling); and rabbit anti-phospho-Chk1 (Ser345) (1:1000, 133D3, Cell Signaling). All Western blotting data are representative for two or three independent experiments.

Immunoprecipitations and *in vitro* kinase assays

Whole-cell extracts were prepared from 10×10^6 cells lysed in buffer containing PBS/10% glycerol/0.1% NP40 and protease inhibitors. Extracts were obtained using 30 µl protein G Sepharose beads (GE Healthcare) incubated with rabbit anti-cyclin A2 antibody (*27*), mouse anti-Cdk2 (1:1000, D-12, sc6248), mouse anti-Cdk1 (1:1000, 610038, BD, rabbit anti-eIF4A2 (1:1000, ab31218, Abcam), or anti-HA affinity matrix (clone 3F10, Roche) overnight at 4°C. Extracts were washed five times in PBS and Western blotting was performed as described above. Kinase assays were as previously described (*28*). Briefly, Cdk2 was immunoprecipitated from MEFs or grinded tumor lysates in PBS with 0.1% NP40 and 10% glycerol supplemented with protease and phosphatase inhibitor cocktails (Roche). Beads were serially washed with kinase buffer (50 mM Tris-HCl, pH 7.7, 100 mM KCl, 5 mM $MgCl_2$, 1 mM DTT, 0.1 mM ATP, and 10 mM β-glycerophosphate) and reactions carried out in the presence of 1 µg histone H1 (EMD Millipore, Cat. No: 14-155) and $\gamma[^{32}P]$ATP. After 45 min at 30°C, reactions were terminated by the addition of Laemmli buffer and analyzed for Histone H1 phosphorylation by SDS-PAGE and autoradiography.

Quantitative real-time PCR

RNA extraction and cDNA synthesis of MEFs were performed as described (*29*). RT-PCR was conducted using SYBR Green (Thermo Fischer Scientific) according to manufacturer's recommendations. The following primers were used for qRT-PCR: *Mre11* forward 5'-AAAGGCTGAGGTGGAGGTCT-3', reverse 5'-AGATTGATGAGGAGGTCCGA-3'; *Rad50* forward 5'-CCGCCAAAGATCACGAATAA-3', reverse 5'-GGTGAACAAGGA CCTCGACA-3'; *Nbs1* forward 5'-AGTTTTTCCTCCCAACAACG-3', reverse 5'-TC ATTTTCAATCAGAATGCCA-3'.

RNA immunoprecipitation and RIP-seq

RNA immunoprecipitation was carried out as described before (*30*), but including an additional step in the beginning that the proteins were crosslinked to nucleic acids by the addition of formaldehyde to growing cells. The immunoprecipitated total RNA was subjected to cDNA synthesis using random hexamers and SuperScript III reverse transcription (Invitrogen), and the cDNAs were used for qRT-PCR analysis of selected transcripts. In addition to the aforementioned *Mre11*, *Rad50* and *Nbs1* qRT-PCR primers, the following primers were used: *Ccna2* forward 5'-GTGGTGATTCAAAACTGCCA-3', reverse 5'-GGCCAGCTGAGCTTAAAGAA-3'. For RIP-seq, 2 cyclin A2 IPs, 2 cyclin E IPs, and 2 rabbit serum controls (IgG-IP) were performed at the same time. For cyclin B1 RIP seq, 2 cyclin B1 IPs, 1 cyclin E IP, and 3 rabbit serum controls (IgG-IP) were performed simultaneously. The RNA from the target IPs and IgG-IPs was converted to cDNA libraries using Ovation RNA-seq system V2 (7102-08, NuGEN) and Ovation Rapid DR Multi-

plex System 1-8 (0319-32, NuGEN). RIP-seq was performed using an Illumina HiSeq 2000 sequencer at the Genomic Core facility of the Mayo Clinic, Rochester, MN. Immunoprecipitation was performed using the following antibodies: rabbit anti-cyclin A2 (*27*) and rabbit anti-cyclin A2 (SC-751, Santa Cruz), anti-HA affinity matrix (clone 3F10, Roche), rabbit anti-cyclin B1 (1:1000, 4138S, Cell Signaling), and rabbit anti-cyclin E (ab7959, Abcam).

mRNA-seq data analysis

mRNA-seq data was processed to identify genes with differential expression among the IP samples. The processing of the mRNA data was performed using MAP-RSeq workflow (v1.2.1.3) (*31*). MAP-RSeq consists of the following steps: alignment, quality control, obtaining genomic features per sample and finally summarizing the data across samples. The pipeline provides detailed quality control data across genes using the RSeQC software (v2.3.2) (*32*). Paired-end reads are aligned by TopHat (*33*) (v2.0.6) against the hg19 genome build using the bowtie1aligner (*34*). Gene counts were generated using HTSeq (*35*) software (v0.5.3p9) and the gene annotation files were obtained from Illumina. Differential expression analysis was performed with edgeR (*36*) package (v2.6.2) to identify genes with altered expression. A cutoff for false discovery rate–adjusted p-value was set at 0.01 to determine the genes with significant expression change between conditions.

Polysome analysis

Polysome analysis was performed as previously described (*37*). Briefly, cells were cultured in 15-cm dishes, and harvested by trypsinization at 80-90% confluence. Cells were lysed with 250 µl polysome lysis buffer (10 mM Tris-HCl [pH 8.0], 140 mM NaCl, 1.5 mM $MgCl_2$, 0.5% NP-40, 200 U of RNasin (Promega)). Extracts were centrifuged in a microcentrifuge for 1 min at 20,000 × *g*. Supernatants were transferred to a fresh microcentrifuge tube and supplemented with 250 µl of 2x translation stop buffer (20 mM dithiothreitol (DTT), 665 µg/ml heparin, 150 µg/ml cycloheximide, and 1 tablet complete protease inhibitor cocktail (Roche) per 5 ml of buffer. Supplemented supernatants were centrifuged for 5 min at 20,000 × *g*. Supernatants (200 µl) were gently layered on top of a 15 to 40% sucrose gradient cast in 10 mM Tris-HCl (pH 7.5), 140 mM NaCl, 1.5 mM $MgCl_2$, 10 mM DTT, 100 µg/ml cycloheximide and 0.5 mg/ml heparin. Gradients were centrifuged in a Beckman ultracentrifuge (TlS 55) for 75 min at 50,000 rpm. Fractions were collected from the top of the gradients and partitioned for RNA isolation. RNA isolation and qRT-PCR were performed as described above.

Luciferase reporter assay

MEFs were transfected with luciferase construct containing SV40 promoter (Promega) and either no Mre11 3'UTR (empty vector), or full-length or various fragments of the Mre11 3'UTR. The cells were also co-transfected with renilla luciferase reporter to be used as an internal control. 24 h after transfection, the cells were harvested for measurement of luciferase activities using a dual luciferase assay kit (Promega, WI). Relative luciferase units were determined by normalizing the firefly activity with the renilla activity.

EMSA

Cyclin $A2^{302-432}$, cyclin $A2^{1-209}$, and mutant cyclin $A2^{302-432}$ carrying mutations in four residues predicted to be critical ribonucleic acid contact sites were subcloned into pGEX-4T to express GST-cyclin A2 fusion proteins. Cyclin $A2^{1-209}$, GST- cyclin $A2^{302-432}$ and GST- mutant cyclin $A2^{302-432}$ were expressed at RT in E. coli strain BL21(DE3) (Agilent Technologies) and purified with glutathione-Sepharose beads (GE Healthcare Life Sciences). His-tagged recombinant human EIF4A2 protein was obtained from Creative Biomart (eIF4A2-47H). All RNA probes (Integrated DNA Technologies) were radioactively labeled using [γ-32P]ATP (20 μCi/probe) and polynucleotide kinase (NEB), as described by the manufacturer. RNA probes (1 nM final concentration) were mixed with the purified proteins in a buffer containing 50 mM Tris pH 7.5, 50 mM NaCl, 1 mM DTT, 1 unit/μl superase (Ambion), 5 mM ribonucleoside vanadyl complex (NEB) and 1x EDTA-free protease inhibitor cocktail (Roche #04693159001), and incubated for 20 min at RT. For supershift assays, various concentrations of the His-tagged EIF4A2 protein were added to the reaction while keeping the amount of cyclin A2 protein constant. Cold competition assays were performed with 200-1600 fold excess of unlabeled RNA probe. Protein-RNA complexes were resolved by electrophoresis through a 4.5% native polyacrylamide gel in 0.5x Tris-borate-EDTA buffer. Complexes were detected and analyzed by storage phosphor technology. RNA oligonucleotides used were as follows: *Mre11* 3'UTR highly conserved C-terminus region 32-mer: GAAUUUUUCUGUUUUCUUAAAAAUACCG-GAAA. Random 32-mer: GCUAU GUACUUAAUGAUAUCACUUGUAAAGUU.

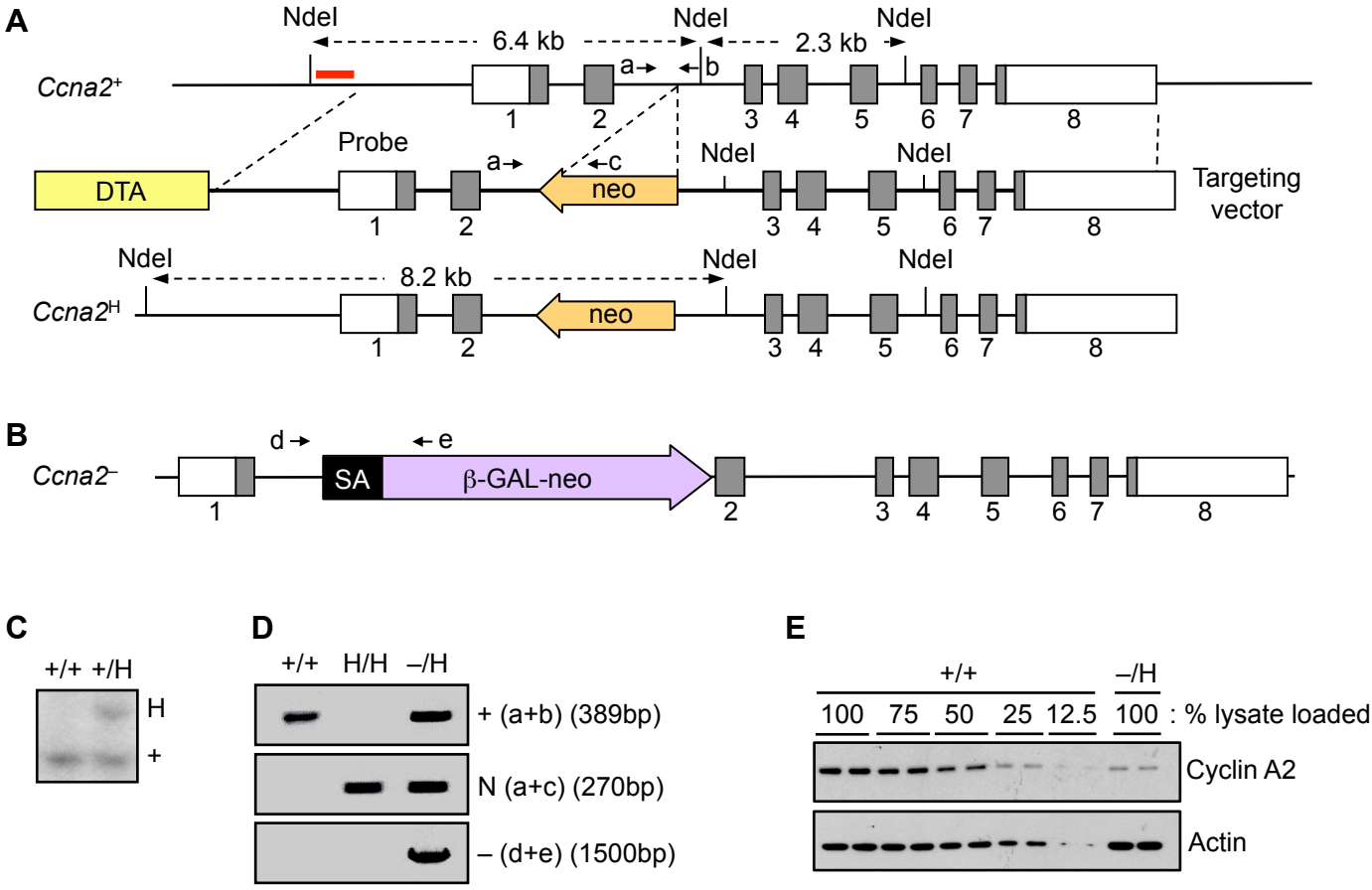

Fig. S1. Generation of cyclin A2 hypomorphic mice. A, Overview of the gene targeting strategy. **B**, *Ccna2*$^{–}$ allele derived from gene trap ES clone DC0194. **C**, Southern blot analysis of mice with the indicated *Ccna2* genotypes. **D**, PCR-based genotype analysis of cyclin A2 mutant mice. Positions of PCR primers a-e are indicated in **A** and **B**. **E**, Estimation of residual cyclin A2 protein in *Ccna2*$^{–/H}$ MEFs.

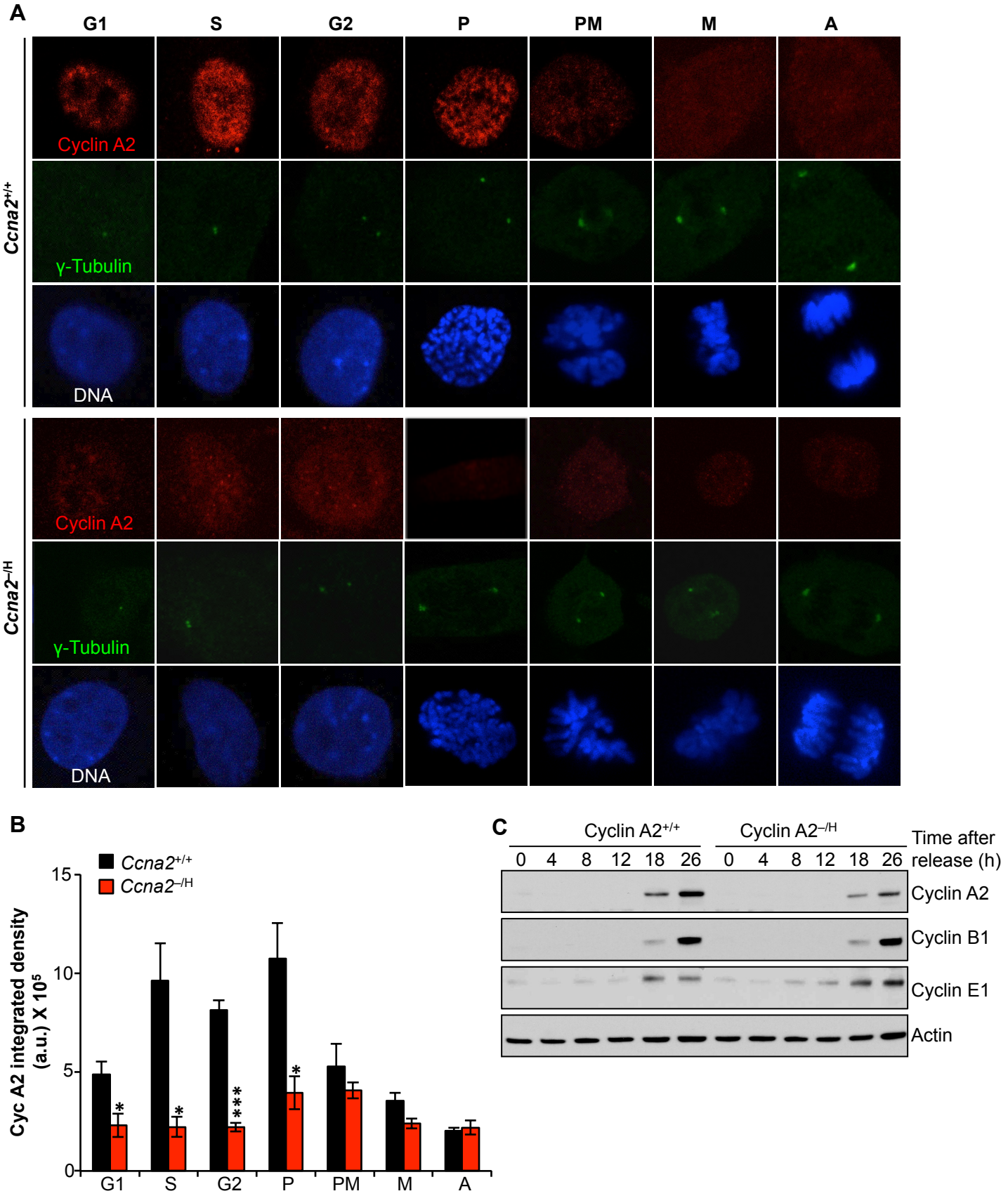

Fig. S2. Cycling *Ccna2*$^{-/H}$ MEFs express low amounts of cyclin A2 during S, G2 and M phase. A, Cyclin A2 immunofluorescence in different cell cycle phases of *Ccna2*$^{+/+}$ and *Ccna2*$^{-/H}$ MEFs. γ-tubulin co-staining was used for cell-cycle staging. **B**, Quantification of cyclin A2 immunofluorescence in different cell cycle phases of *Ccna2*$^{+/+}$ and *Ccna2*$^{-/H}$ MEFs. **C,** Levels of core cyclins during cell-cycle progression. MEFs were arrested in G_0 by serum deprivation for 18 h and collected at the indicated times after adding serum for assessment of cyclin levels using western blot analysis. *Ccna2*$^{-/H}$ MEFs show reduced cyclin A2 and increased cyclin E1 levels. Data shown are the mean of 3 independent cell lines per genotype. In **B**, at least 10 cells per line for each cell cycle phase. Error bars represent SEM. Statistical significance was determined by an unpaired *t*-test. *$P < 0.05$, ***$P < 0.001$.

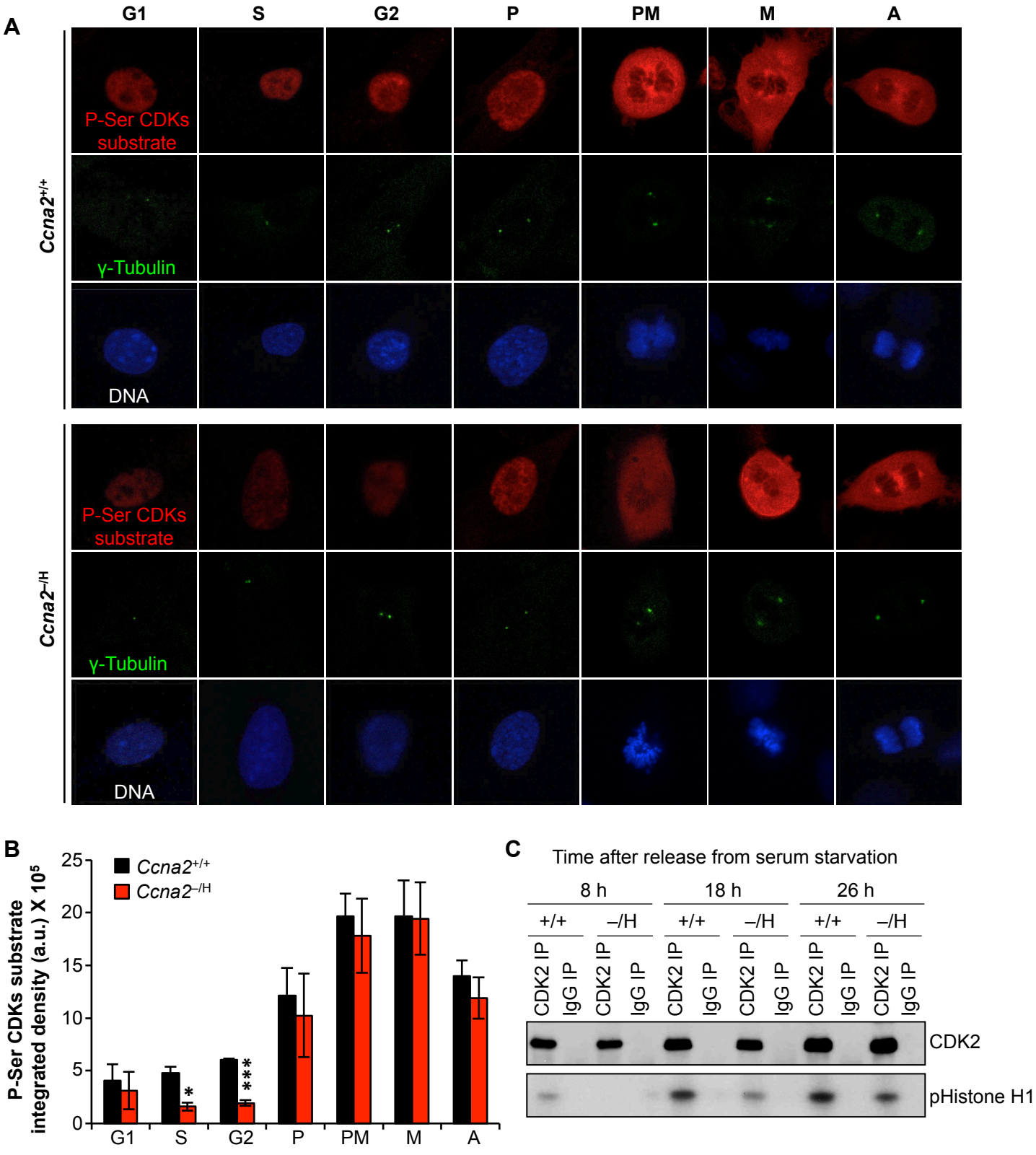

Fig. S3. Cdk-dependent substrate phosphorylation is reduced during S and G2 phase. A, Immunodetection of phosphorylated Cdk-substrates in different cell cycle phases of *Ccna2*$^{+/+}$ and *Ccna2*$^{-/H}$ MEFs. g-tubulin co-staining was used for cell-cycle staging. **B**, Quantification of phosphorylated Cdk-substrates signals in *Ccna2*$^{+/+}$ and *Ccna2*$^{-/H}$ MEFs. **C**, Measurement of Cdk2 kinase activity in *Ccna2*$^{+/+}$ and *Ccna2*$^{-/H}$ MEFs at various time points after release from serum starvation by immunoprecipitating Cdk2 from MEF lysates and incubating it in the presence of histone H1 and γ[^{32}P]ATP. Data shown in **B** are the mean of 3 independent lines per genotype (at least 10 cells per line for each cell cycle phase) and error bars represent SEM. Statistical significance was determined by an unpaired *t*-test. **P* < 0.05, ****P* < 0.001.

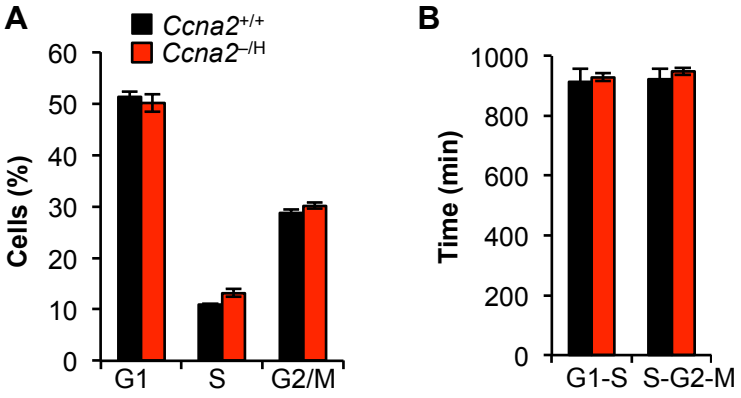

Fig. S4. Cyclin A2 insufficiency does not impact timing of cell-cycle phases. A, Cell-cycle profiles of propidium iodide-stained *Ccna2*$^{+/+}$ and *Ccna2*$^{–/H}$ MEFs analyzed by flow cytometry. N = 3 independent MEF lines per genotype). **B**, Cell cycle distribution of *Ccna2*$^{+/+}$ and *Ccna2*$^{–/H}$ MEFs analyzed by FUCCI. Error bars represent SEM. *N* = 3 independent MEF lines per genotype (at least 5 cells were analyzed per line).

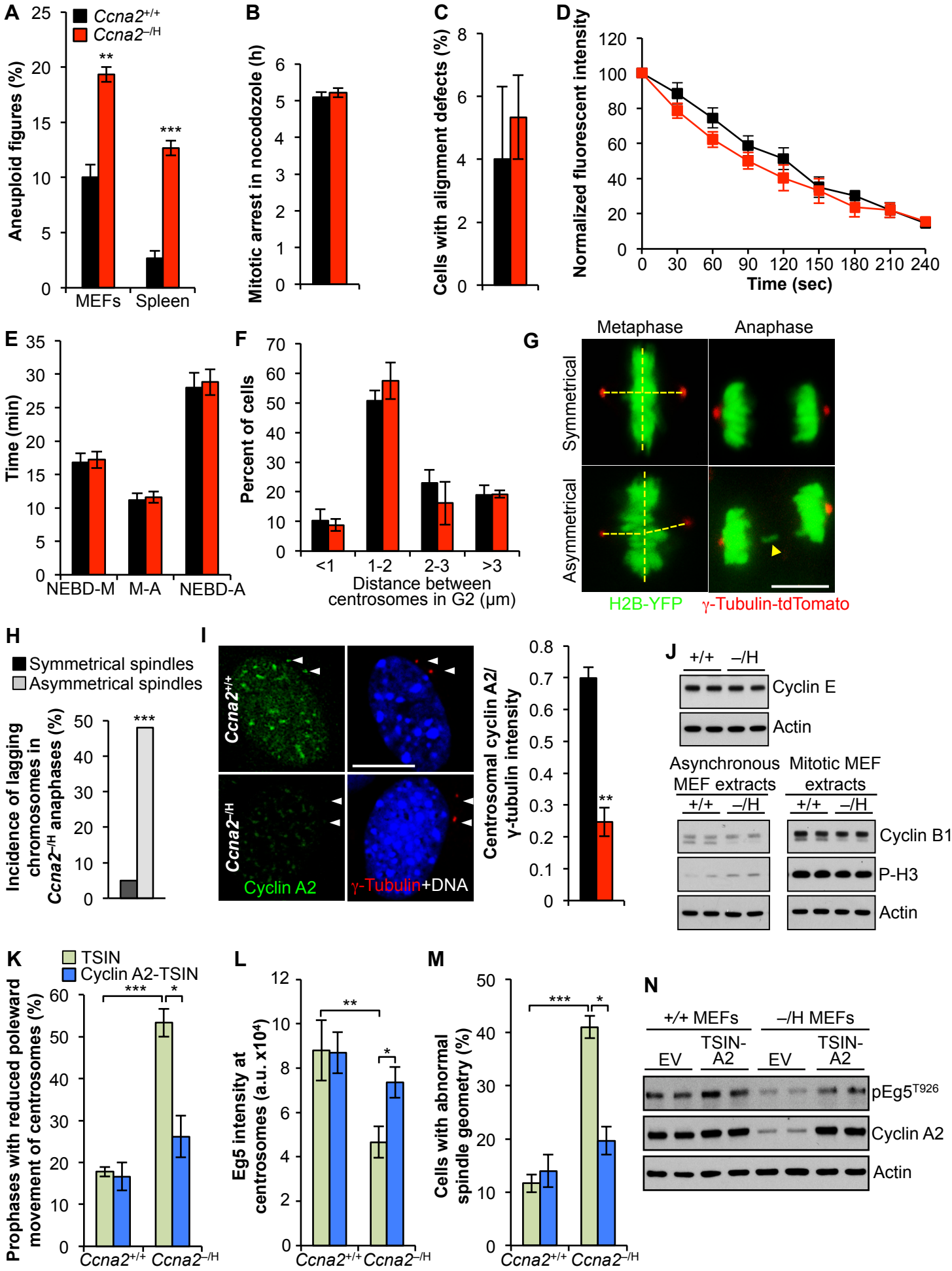
A
Ccna2+/+
Ccna2–/H
Aneuploid figures (%)
MEFs
Spleen
B
Mitotic arrest in nocodozole (h)
C
Cells with alignment defects (%)
D
Normalized fluorescent intensity
Time (sec)
E
Time (min)
NEBD-M
M-A
NEBD-A
F
Percent of cells
Distance between centrosomes in G2 (μm)
G
Metaphase
Anaphase
Symmetrical
Asymmetrical
H2B-YFP
γ-Tubulin-tdTomato
H
Symmetrical spindles
Asymmetrical spindles
Incidence of lagging chromosomes in Ccna2–/H anaphases (%)
I
Cyclin A2
γ-Tubulin+DNA
Centrosomal cyclin A2/ γ-tubulin intensity
J
Cyclin E
Actin
Asynchronous MEF extracts
Mitotic MEF extracts
Cyclin B1
P-H3
K
TSIN
Cyclin A2-TSIN
Prophases with reduced poleward movement of centrosomes (%)
L
Eg5 intensity at centrosomes (a.u. x10⁴)
M
Cells with abnormal spindle geometry (%)
N
+/+ MEFs
–/H MEFs
EV
TSIN-A2
pEg5T926
Cyclin A2
Actin

Fig. S5. Analyses of cyclin A2 insufficient cells for causes of chromosome missegregation. A, Karyotype analysis of P5 MEFs and splenocytes from 5-month-old mice (3 lines per genotype and 50 spreads per line). **B**, Measurement of mitotic checkpoint activity using a nocodozole-challenge assay. **C**, Analysis of the error correction machinery using a monastrol washout assay. **D**, Measurement of kinetochore-microtubule attachment stability using ectopically expressed photo-activatable GFP-α-tubulin protein. Normalized fluorescent intensity over time after photo-activation of spindle in prometaphase cells. We analyzed 3 independent lines per genotype (5 cells per line). **E**, Live-cell imaging analysis of mitotic timing in H2B-mRFP expressing *Ccna2*$^{+/+}$ and *Ccna2*$^{-/H}$ MEFs (3 independent lines per genotype; at least 20 cells were analyzed per line). **F**, Measurement of centrosome separation in G2 cells (3 independent lines per genotype; at least 10 cells were analyzed per line). **G**, Still images of *Ccna2*$^{-/H}$ MEFs monitored by live-cell microscopy illustrating that metaphases with misaligned spindle poles (reflective of spindle asymmetry) transition into anaphases with lagging chromosomes (metaphases shown were images taken just prior to anaphase onset). **H**, Incidence of chromosome lagging in metaphases with symmetrical and asymmetrical spindles. $N = 75$ symmetrical and 25 asymmetrical spindles. **I**, MEFs immunostained for cyclin A2 (green), γ-tubulin (red), and Hoechst (blue). Quantification of cyclin A2 signals at centrosomes (3 independent lines per genotype; at least 10 cells were analyzed per line). **J**, Immunoblots of MEF lysates probed with antibodies for cyclin E and cyclin B. Actin and P-H3 were used as loading controls. **K**, Incidence of prophases with delayed centrosome movement in TSIN (empty vector) or cyclin A2-TSIN transduced MEFs (3 independent lines per genotype; at least 10 cells we analyzed per line). **L**, Quantification of Eg5 signal at centrosomes in prophase of TSIN or cyclin A2-TSIN transduced MEFs. (3 independent lines per genotype; at least 10 cells were analyzed per line). **M**, Percentage of metaphase cells with abnormal spindle geometry in TSIN or cyclin A2-TSIN expressing MEFs. (3 independent lines per genotype; at least 10 cells we analyzed per line). **N,** Immunoblot analysis of phospho-Eg5^{T926} and cyclin A2 in *Ccna2*$^{+/+}$ and *Ccna2*$^{-/H}$ MEFs expressing TSIN (empty vector) or cyclin A2-TSIN. Actin was used as loading control. Error bars represent SEM. Scale bars in **G** and **I** are 10 μm. Statistical significance was determined by an unpaired *t*-test, except for **G** where a Fisher's exact test was used. $*P < 0.05$, $**P < 0.01$, $***P < 0.001$.

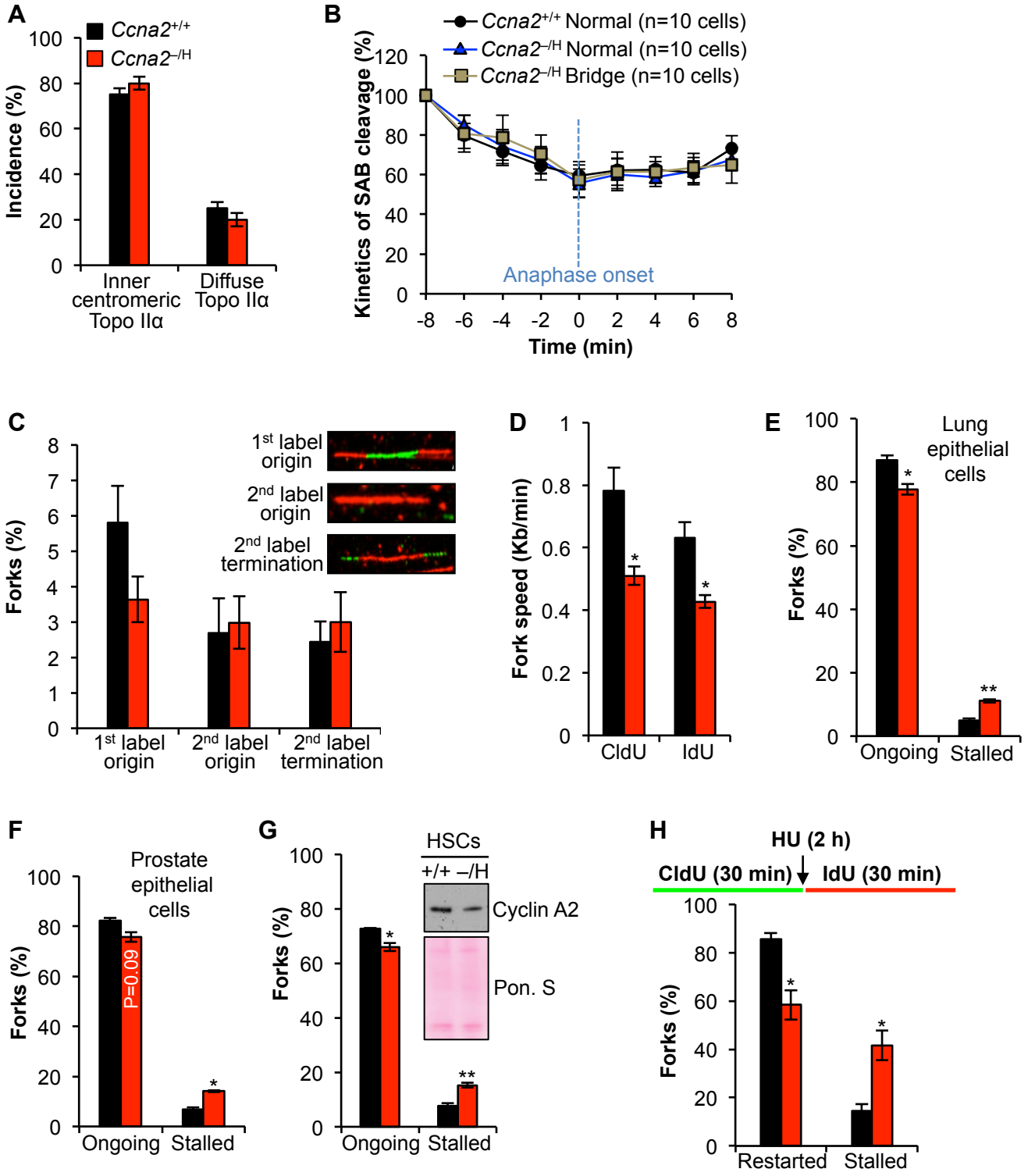

Fig. S6. Cyclin A2 insufficiency causes DNA replication errors and DSBs irrespective of cell type. A, Quantification of inner centromeric and diffused localization of TopoIIα in prometaphase of *Ccna2*$^{+/+}$ and *Ccna2*$^{-/H}$ MEFs. **B**, Kinetics of separase cleavage in MEFs. **C**, Quantification of replication forks as in Fig. 3A, but showing forks of first label origin (red-green-red), second label origin (red only), and second label termination (green-red-green). **D**, Distribution of replication fork speed (CldU and IdU, > 60 fibers per cell line. $N = 3$ independent cell lines per genotype). **E-G**, Percentage of progressing and stalled replication forks in murine lung (**E**) and prostate epithelial cells (**F**), and hematopoietic stem cells (**G**) ($N = 3$ independent lines per genotype; at least 100 fibers were analyzed per line). Inset in **G** shows an immunoblot of hematopoietic stem cell lysates probed for cyclin B. **H**, Quantification of restarted replication forks after 2 h hydroxyurea (HU) treatment in *Ccna2*$^{+/+}$ and *Ccna2*$^{-/H}$ MEFs. A schematic of labeling and treatment protocol is shown at the top of the graph. Error bars represent SEM. Statistical significance was determined by an unpaired *t*-test. *$P < 0.05$, **$P < 0.01$.

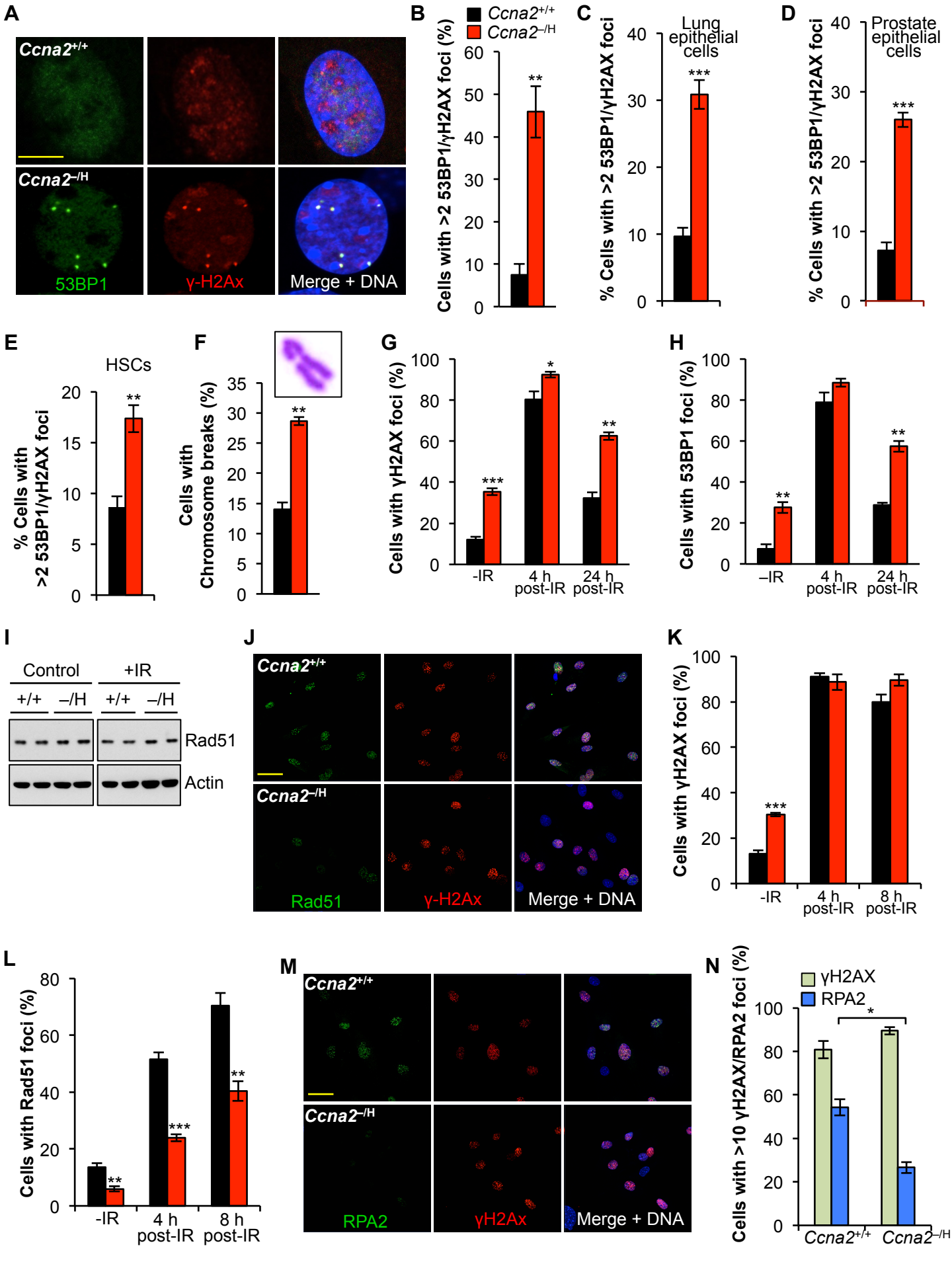
A
Ccna2+/+
Ccna2–/H
53BP1
γ-H2Ax
Merge + DNA
B
Ccna2+/+
Ccna2–/H
Cells with >2 53BP1/γH2AX foci (%)
C
Lung epithelial cells
% Cells with >2 53BP1/γH2AX foci
D
Prostate epithelial cells
% Cells with >2 53BP1/γH2AX foci
E
HSCs
% Cells with >2 53BP1/γH2AX foci
F
Cells with Chromosome breaks (%)
G
Cells with γH2AX foci (%)
-IR
4 h post-IR
24 h post-IR
H
Cells with 53BP1 foci (%)
–IR
4 h post-IR
24 h post-IR
I
Control
+IR
+/+
–/H
+/+
–/H
Rad51
Actin
J
Ccna2+/+
Ccna2–/H
Rad51
γ-H2Ax
Merge + DNA
K
Cells with γH2AX foci (%)
-IR
4 h post-IR
8 h post-IR
L
Cells with Rad51 foci (%)
-IR
4 h post-IR
8 h post-IR
M
Ccna2+/+
Ccna2–/H
RPA2
γH2Ax
Merge + DNA
N
γH2AX
RPA2
Cells with >10 γH2AX/RPA2 foci (%)
Ccna2+/+
Ccna2–/H

Fig. S7. Repair of radiation-induced DSBs is impaired when cyclin A2 is low. A, Images of *Ccna2*$^{+/+}$ and *Ccna2*$^{-/H}$ MEFs immunostained for γH2AX and 53BP1 co-localized foci. **B-E**, Quantification of cells with >2 γH2AX-53BP1 double positive foci in MEFs (**B**) and lung (**C**) and prostate epithelial cells (**D**), and hematopoietic stem cells (**E**). $N = 3$ independent lines per genotype; at least 100 cells were analyzed per line. **F**, Quantification of chromosome breaks in metaphase spread of *Ccna2*$^{+/+}$ and *Ccna2*$^{-/H}$ P5 MEFs. Representative image of chromosome break is shown at the top of the graph. **G**, Quantification of cells with >5 γH2AX foci before and 4 h or 24 h after 5 Gy γ-irradiation. **H**, Quantification of cells with >5 53BP1 foci in non-irradiated and at 4 h and 24 h after 5 Gy γ-irradiation. **I,** Immunoblot of *Ccna2*$^{+/+}$ and *Ccna2*$^{-/H}$ MEF lysates probed for Rad51. **J**, Immunofluorescence of *Ccna2*$^{+/+}$ and *Ccna2*$^{-/H}$ MEFs stained with γH2AX and Rad51 at 8 h after 5 Gy γ-irradiation. **K**, Quantification of cells with >5 γH2AX foci prior to and 4 h and 8 h after 5 Gy γ-irradiation. **L**, Quantification of cells with >10 γH2AX and Rad51 co-localized foci. **M**, Immunofluorescence of *Ccna2*$^{+/+}$ and *Ccna2*$^{-/H}$ MEFs stained with γH2AX and RPA2 at 4 h after 10 Gy γ-irradiation. **N**, Quantification of cells with >10 γH2AX and RPA co-localized foci at 4 h after 10 Gy γ-irradiation. γH2AX marks the DSBs and RPA marks resection. $N = 3$ independent lines per genotype in **F-H**, **K**, **L** and **N**. Error bars represent SEM. Statistical significance was determined by an unpaired *t*-test. *$P < 0.05$, **$P < 0.01$, ***$P < 0.001$.

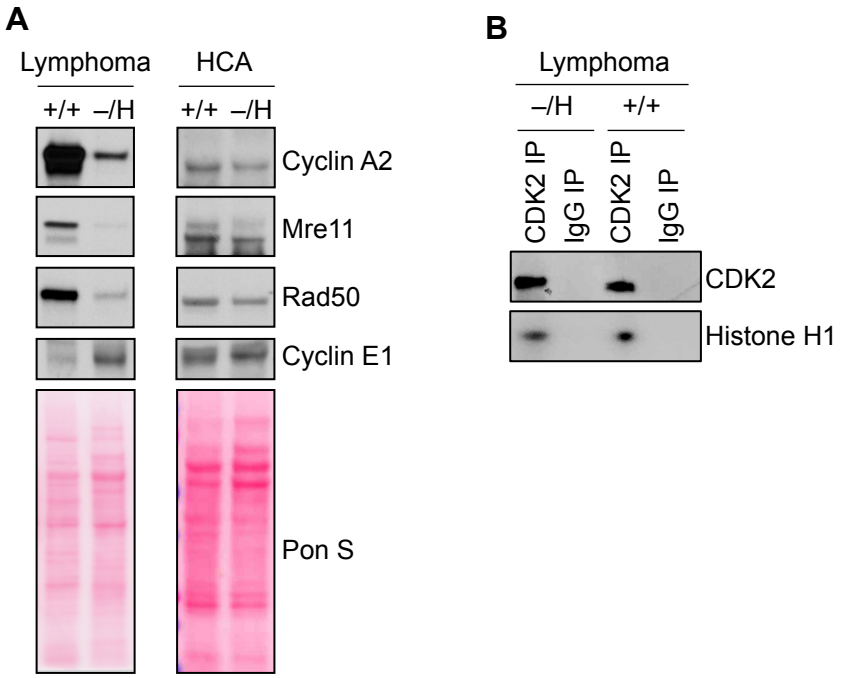

Fig. S8. *Ccna2*$^{-/H}$ tumors exhibit reduced levels of cyclin A2, Mre11 and Rad50 but normal Cdk2 activity. A, Immunoblot of lymphoma and hepatocellular adenoma (HCA) lysates from *Ccna2*$^{+/+}$ and *Ccna2*$^{-/H}$ mice. **B**, Measurement of Cdk2 kinase activity in *Ccna2*$^{+/+}$ and *Ccna2*$^{-/H}$ lymphomas shown in **A**. Cdk2 was immunoprecipitated from lymphoma lysates and incubated with histone H1 in the presence of γ[^{32}P]ATP.

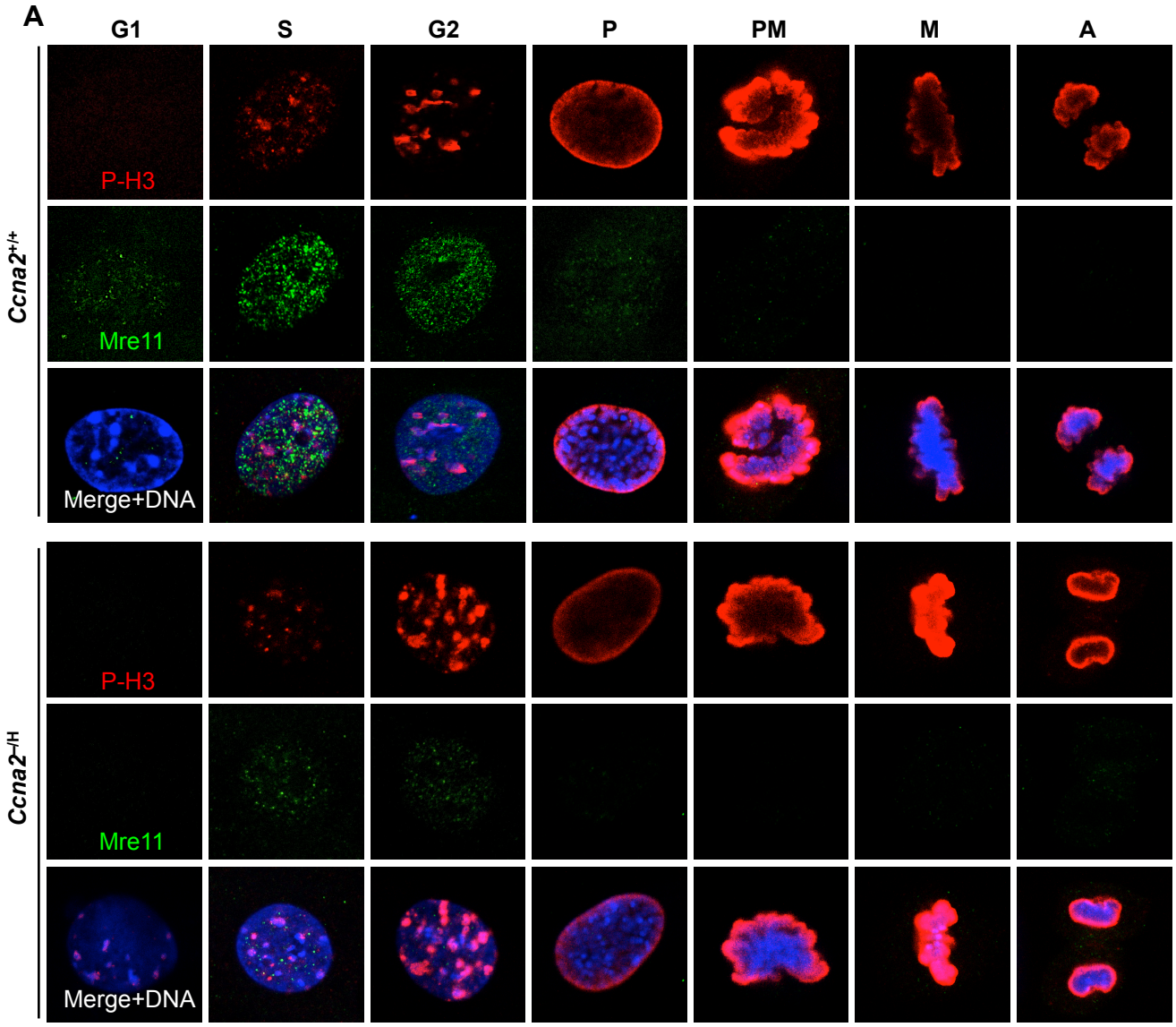

Fig. S9. Cycling cells markedly increase Mre11 expression during S and G2 phase. A, Immunodetection of Mre11 in *Ccna2*$^{+/+}$ and *Ccna2*$^{-/H}$ MEFs at different cell-cycle stages. P-H3 co-staining was used for cell-cycle staging as previously described . **B**, Quantification of Mre11 signals of *Ccna2*$^{+/+}$ and *Ccna2*$^{-/H}$ MEFs in various stages of the cell cycle. Data shown are the mean of 3 independent cell lines per genotype (>10 cells per line for each cell cycle stage). Error bars represent SEM. Statistical significance was determined by an unpaired *t*-test. *$P < 0.05$, **$P < 0.01$.

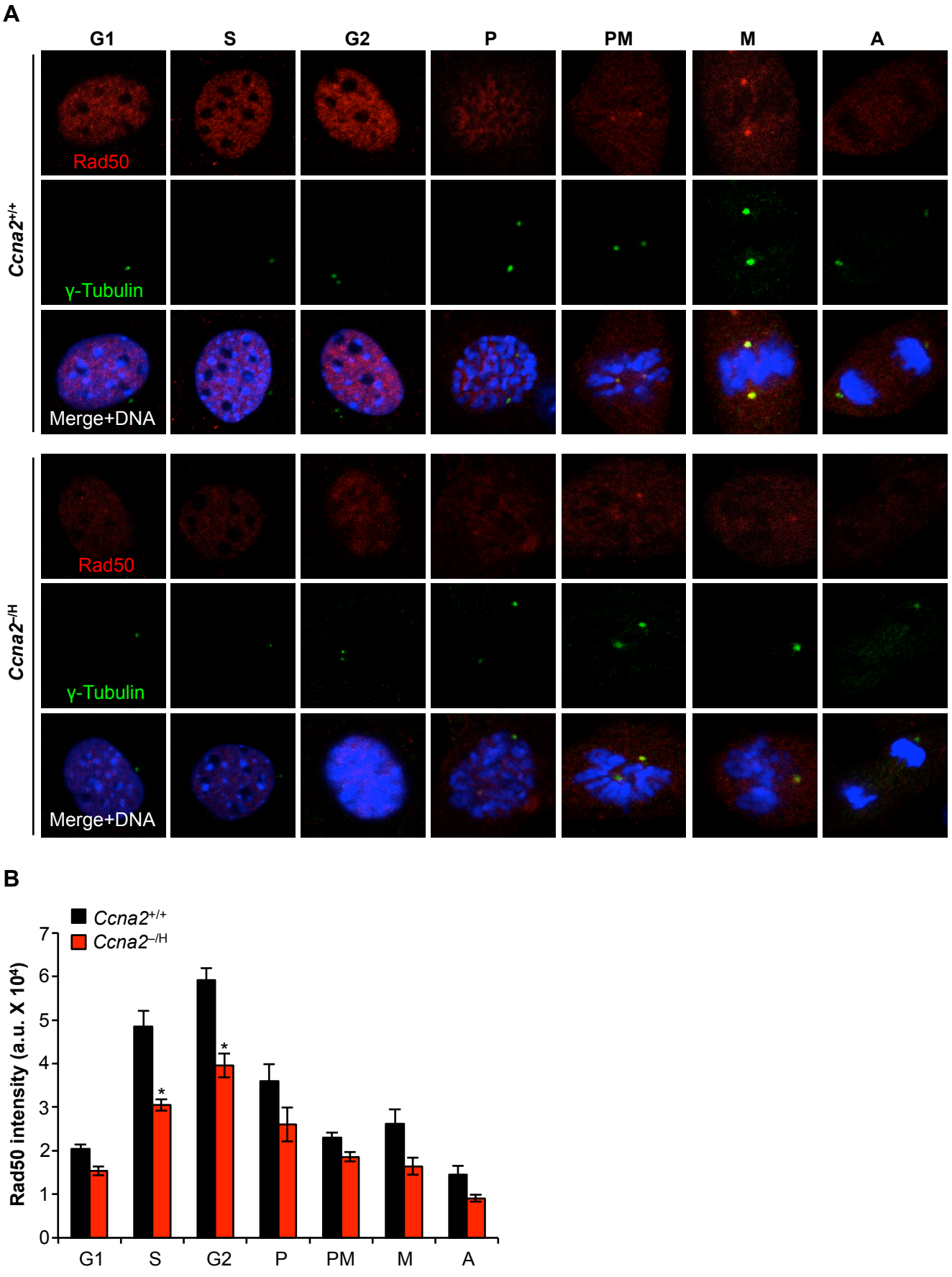

Fig. S10. Cycling cells have increased levels of Rad50 during S and G2 phase. A, Immunodetection of Rad50 in *Ccna2*$^{+/+}$ and *Ccna2*$^{-/H}$ MEFs at different cell-cycle stages. **B**, Quantification of Rad50 immunofluorescence in different cell cycle phases of *Ccna2*$^{+/+}$ and *Ccna2*$^{-/H}$ MEFs. Data shown are the mean of 3 independent cell lines per genotype (>10 cells per line for each cell cycle phase). Error bars represent SEM. Statistical significance was determined by an unpaired *t*-test. *$P < 0.05$.

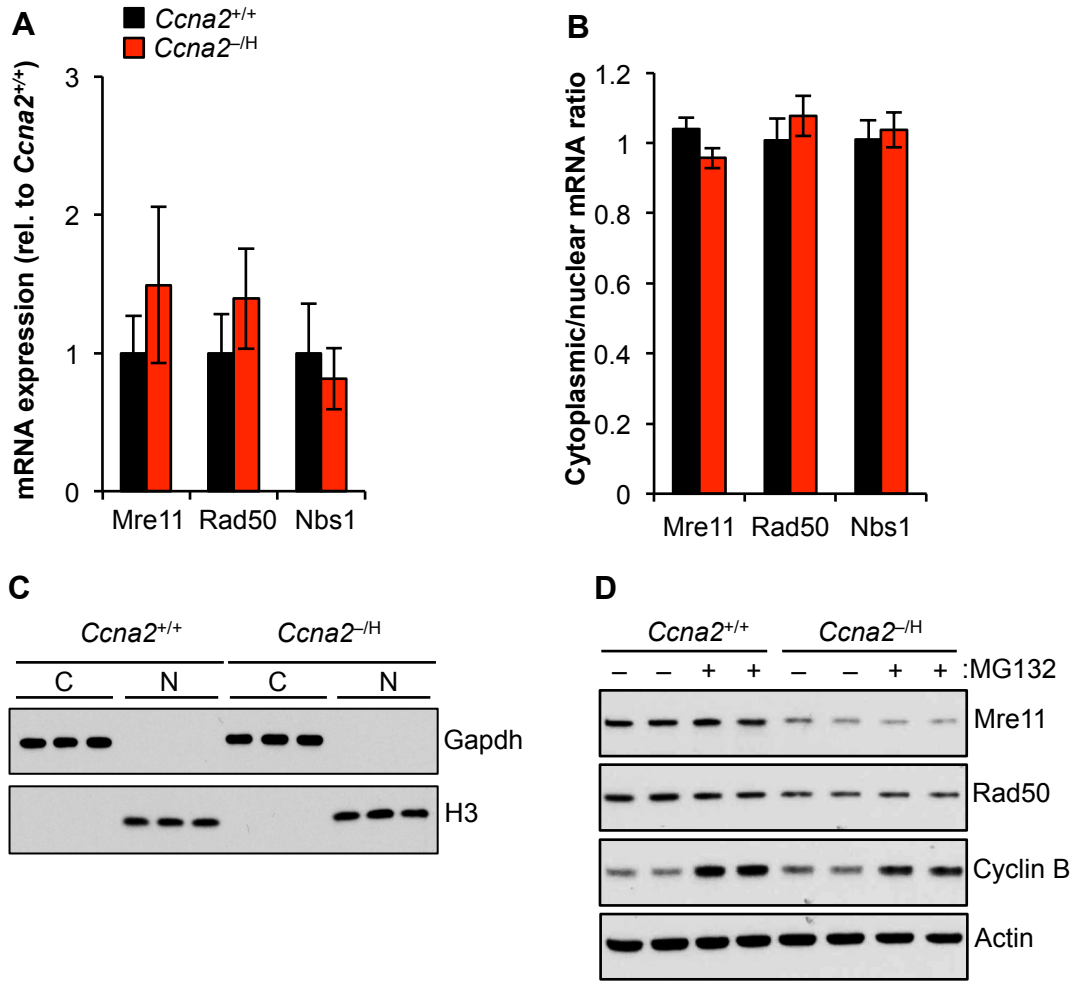

Fig. S11. Low Mre11 and Rad50 levels in *Ccna2*$^{-/H}$ cells are not due to changes in nuclear export of mRNA or proteosomal degradation. A, qRT-PCR analysis of indicated mRNAs in *Ccna2*$^{+/+}$ and *Ccna2*$^{-/H}$ MEFs. **B**, qRT-PCR analysis of indicated mRNAs in cytoplasmic (C) and nuclear (N) fractions of *Ccna2*$^{+/+}$ and *Ccna2*$^{-/H}$ MEFs. **C**, Immunoblots of cytoplasmic (C) and nuclear (N) fractions used in **A** probed for GAPDH (cytoplasmic) and P-H3 (nuclear) to verify the accuracy of the cell fractionation process. **D**, Immunoblots of lysates prepared from *Ccna2*$^{+/+}$ and *Ccna2*$^{-/H}$ MEFs prior to and following 1 h of MG132 treatment probed for Mre11, Rad50, and cyclin B1. Error bars represent SEM. $N = 3$ independent lines per genotype.

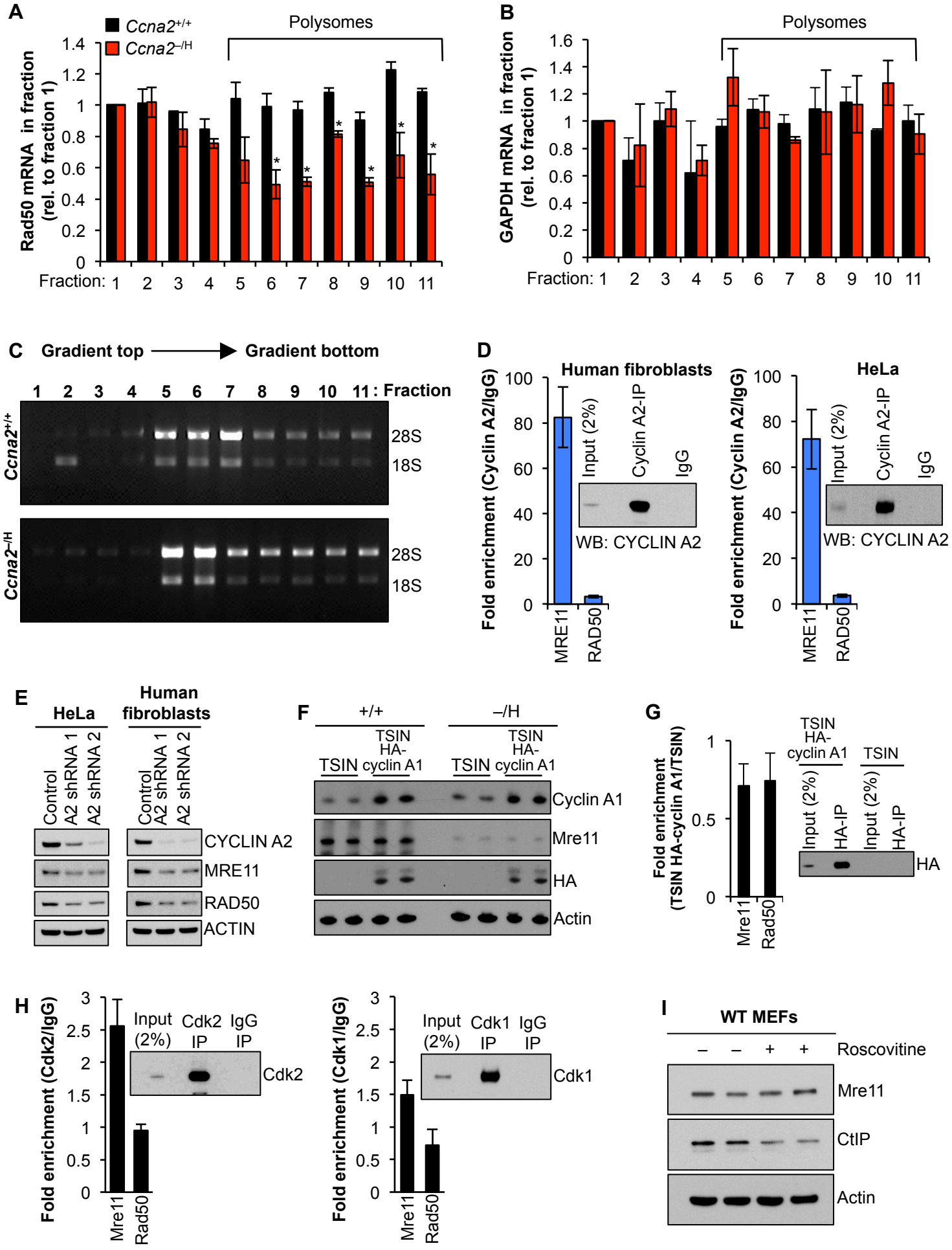
A
Ccna2+/+
Ccna2–/H
Polysomes
Rad50 mRNA in fraction (rel. to fraction 1)
Fraction: 1 2 3 4 5 6 7 8 9 10 11
B
Polysomes
GAPDH mRNA in fraction (rel. to fraction 1)
Fraction: 1 2 3 4 5 6 7 8 9 10 11
C
Gradient top
Gradient bottom
1 2 3 4 5 6 7 8 9 10 11 : Fraction
Ccna2+/+
28S
18S
Ccna2–/H
28S
18S
D
Human fibroblasts
HeLa
Fold enrichment (Cyclin A2/IgG)
Input (2%)
Cyclin A2-IP
IgG
WB: CYCLIN A2
MRE11
RAD50
E
HeLa
Human fibroblasts
Control
A2 shRNA 1
A2 shRNA 2
CYCLIN A2
MRE11
RAD50
ACTIN
F
+/+
–/H
TSIN
TSIN HA-cyclin A1
Cyclin A1
Mre11
HA
Actin
G
Fold enrichment (TSIN HA-cyclin A1/TSIN)
TSIN HA-cyclin A1
TSIN
Input (2%)
HA-IP
HA
Mre11
Rad50
H
Fold enrichment (Cdk2/IgG)
Input (2%)
Cdk2 IP
IgG IP
Cdk2
Fold enrichment (Cdk1/IgG)
Input (2%)
Cdk1 IP
IgG IP
Cdk1
Mre11
Rad50
I
WT MEFs
Roscovitine
Mre11
CtIP
Actin

Fig. S12. Cyclin A2 binds to *Mre11* transcripts in a Cdk-independent fashion in both human and mouse cells. A and **B**, Quantification of *Rad50* (**A**) and *GAPDH* mRNA (**B**) in polysome fractions of *Ccna2*$^{+/+}$ and *Ccna2*$^{-/H}$ MEFs. **C**, Agarose gel electrophoresis of sucrose gradient fractions from *Ccna2*$^{+/+}$ and *Ccna2*$^{-/H}$ MEFs to show fractions containing polysomes (fractions containing 28S and 18S rRNA). **D**, RNA immunoprecipitation with cyclin A2 antibody on primary human foreskin fibroblasts or HeLa cells. **E**, Western blots of lysates from human fibroblasts or HeLa cells transduced with independent cyclin A2 shRNAs or non-targeting shRNA negative control lentiviruses and probed for the indicated proteins. **F**, Immunoblot analysis of *Ccna2*$^{+/+}$ and *Ccna2*$^{-/H}$ MEFs transduced with TSIN or HA-cyclin A1-TSIN lentiviruses. Actin was used as loading control. **G**, RNA immunoprecipitation for HA on *Ccna2*$^{+/+}$ MEFs transduced with HA-cyclin A1-TSIN or TSIN lentiviruses. Insets show immunoblots of the amounts of Cdk1 and Cdk2 immunoprecipitated with specific and control antibodies. **H**, RNA immunoprecipitation analysis with Cdk1 and Cdk2 antibody on *Ccna2*$^{+/+}$ MEFs. Insets shows an immunoblots of immunoprecipitated of Cdk1 and Cdk2 with specific and control antibodies. **I**, Immunoblots of lysates from *Ccna2*$^{+/+}$ MEFs cultured in the absence or presence of 10 μM roscovitine for 48 h. Error bars represent SEM. $N = 3$ independent MEF lines per genotype except for **D** where $N = 3$ independent experiments with human fibroblasts or HeLa cells.

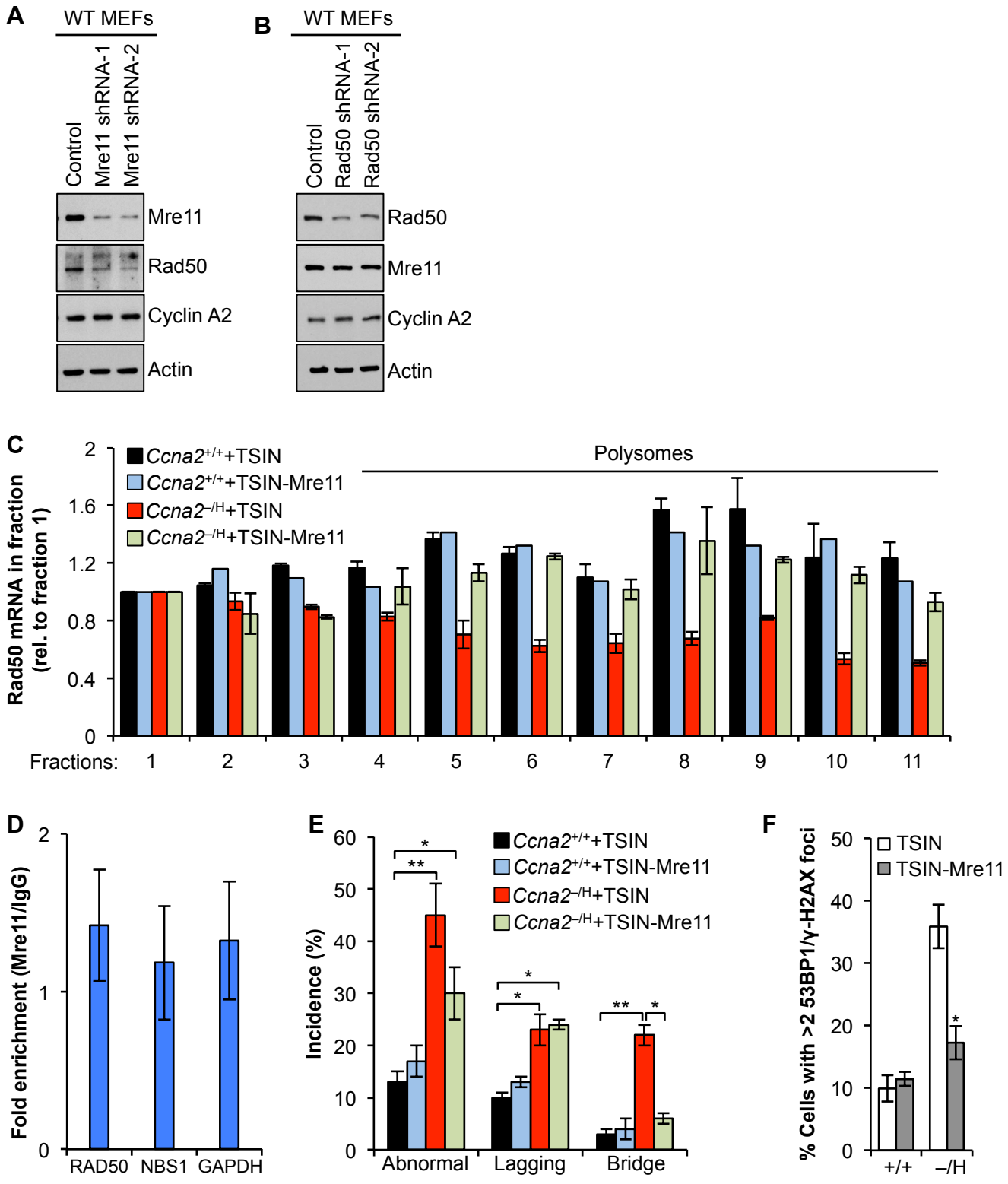

Fig. S13. *Rad50* mRNA translation is Mre11 dependent. A, Western blot of indicated proteins after Mre11 knock-down in *Ccna2*$^{+/+}$ MEFs. **B**, Western blot of indicated proteins after Rad50 knock-down in *Ccna2*$^{+/+}$ MEFs. **C**, Quantification of *Rad50* mRNA in polysome fractions of *Ccna2*$^{+/+}$ and *Ccna2*$^{-/H}$ MEFs transduced with TSIN or TSIN-*Mre11* lentivirus. **D**, RNA immunoprecipitation analysis using Mre11 antibody in primary human fibroblast cells. **E**, Live-cell imaging of *Ccna2*$^{+/+}$ and *Ccna2*$^{-/H}$ MEFs expressing Mre11 progressing through and unchallenged mitosis. **F**, Quantification of cells with >2 γH2AX and 53BP1 co-localized foci in *Ccna2*$^{+/+}$ and *Ccna2*$^{-/H}$ MEFs infected with Mre11-containing or control lentiviruses. Error bars represent SEM. $N = 3$ independent MEF lines per genotype. Statistical significance was determined by an unpaired *t*-test. *$P < 0.05$, **$P < 0.01$.

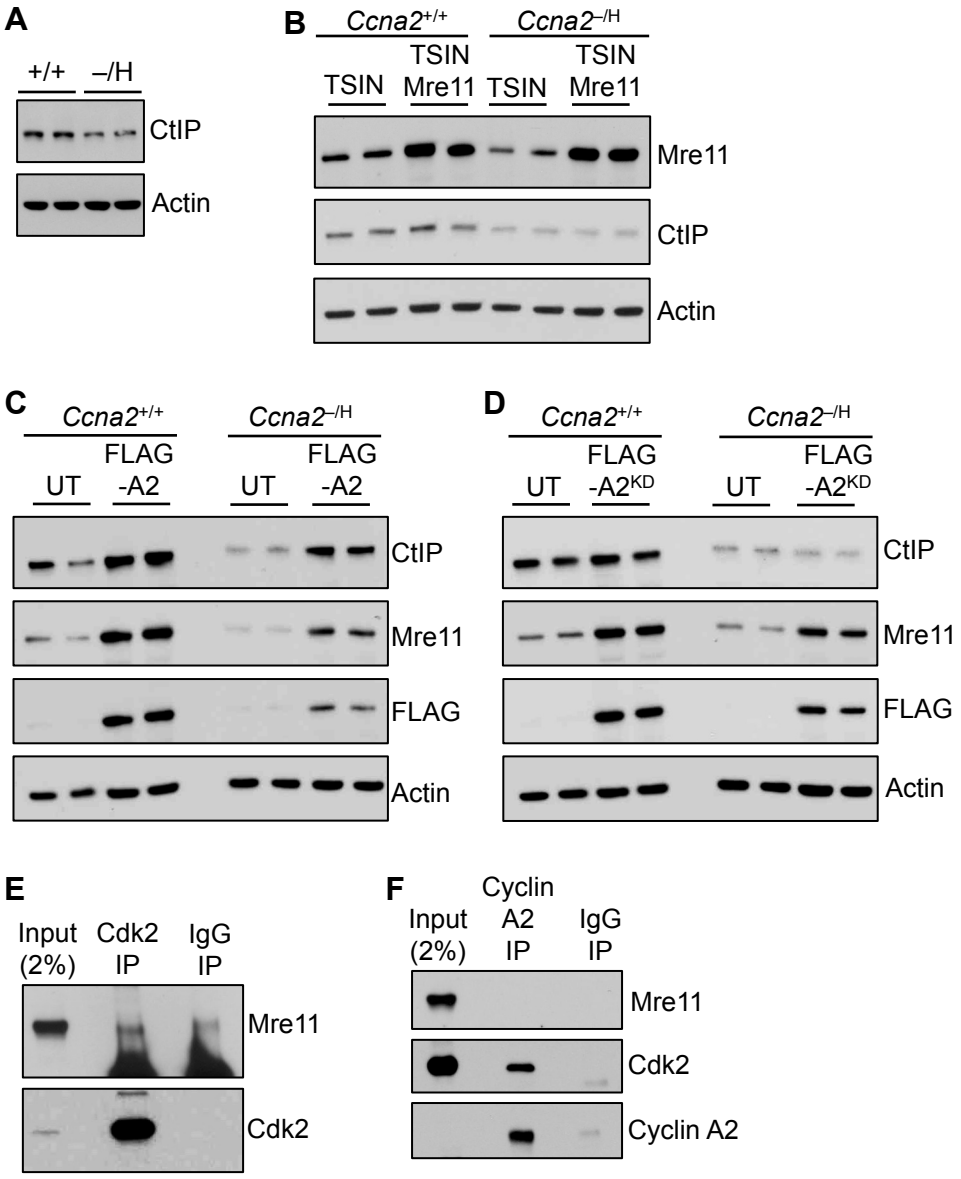

Fig. S14. CtIP protein levels are cyclin A2-Cdk dependent. A, Western blot analysis of MEF lysates probed for CtIP. **B** and **C**, Immunoblots of *Ccna2*$^{+/+}$ and *Ccna2*$^{-/H}$ MEFs transduced with lentivirus expressing FLAG-tagged wild-type cyclin A2 or mutant cyclin A2 containing a point mutation that precludes Cdk binding, probed for the indicated antibodies. Note that wild-type cyclin A2 and non-Cdk binding cyclin A2 mutant both rescued Mre11 expression, however, only wild-type cyclin A2 rescued CtIP, indicating that cyclin A2/Cdk activity is critical for maintaining normal CtIP levels. **D**, Immunoblots of *Ccna2*$^{+/+}$ and *Ccna2*$^{-/H}$ MEFs transfected with Mre11 expression construct. Consistent with the results in **B** and **C**, Mre11 expression alone did not rescue CtIP abundance in hypomorphic MEFs. **E**, and **F**, Immunoprecipitation experiments performed to explore whether Mre11 interacts with cyclin A2-Cdk2. **E**, Immunoblots of wild-type MEF extracts subjected to immunoprecipitation with Cdk2 antibody or control IgG and analyzed with Mre11 and Cdk2. **F**, Immunoblots of wild-type MEF extracts subjected to immunoprecipitation with cyclin A2 antibody or control IgG and analyzed with Mre11, Cdk2, and cyclin A2. These binding studies were unable to confirm earlier work documenting that Mre11 interacts with cyclin A2-Cdk2 (*38*).

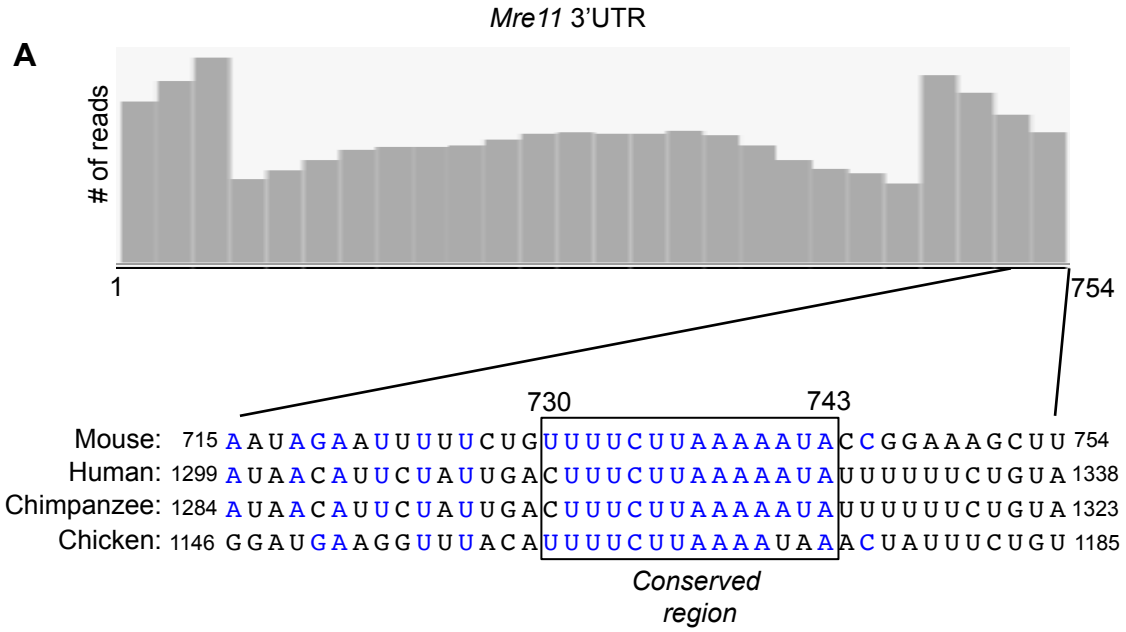

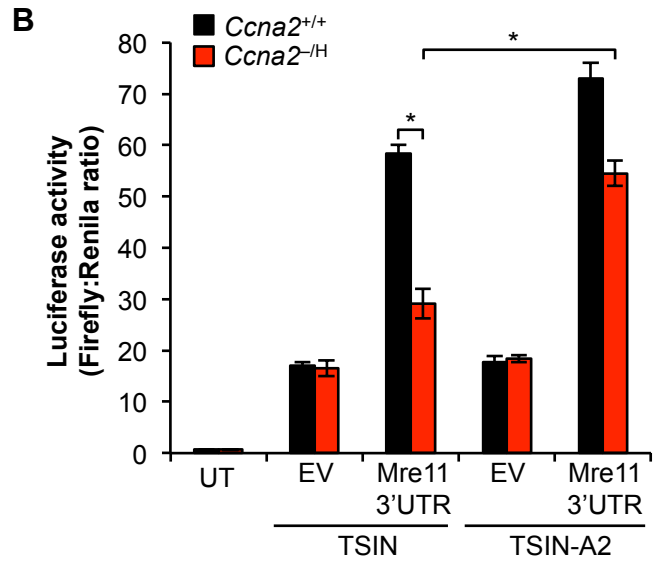

Fig. S15. RNA sequencing reads mapping to the *Mre11* 3'UTR. A, Sequence alignment of the 3' end of the *Mre11* 3'UTRs of the indicated species. A highly conserved region is boxed. **B**, Luciferase activity in cyclin A2 expressing MEFs transfected with 3'UTR of *Mre11* mRNA. UT, untransfected; EV, empty vector. Error bars represent SEM. $N = 3$ independent MEF lines per genotype. Statistical significance was determined by an unpaired *t*-test. $*P < 0.05$.

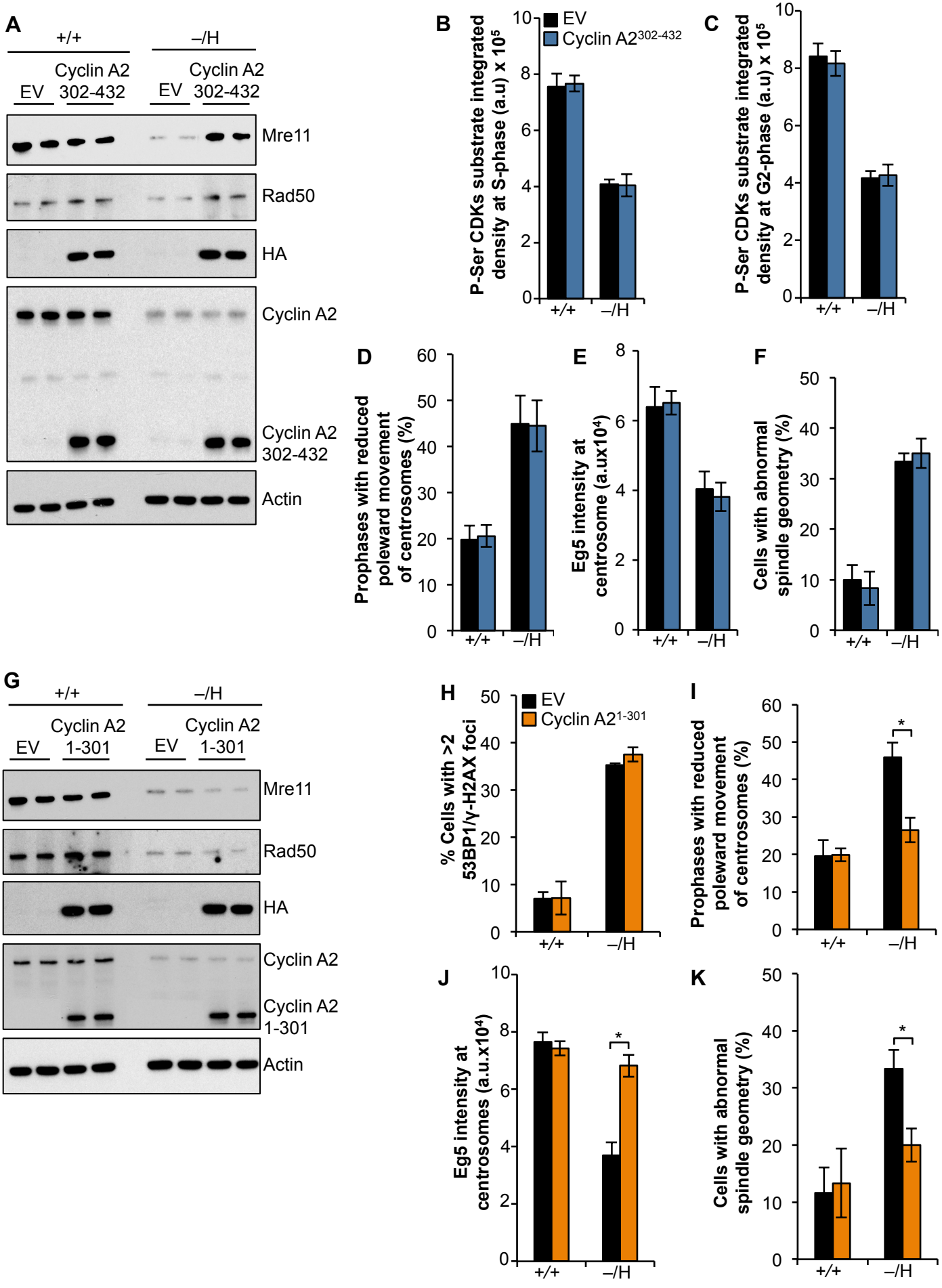
A
+/+
–/H
Cyclin A2
EV
302-432
EV
Cyclin A2
302-432
Mre11
Rad50
HA
Cyclin A2
Cyclin A2
302-432
Actin
B
EV
Cyclin A2302-432
P-Ser CDKs substrate integrated density at S-phase (a.u) x 10⁵
+/+
–/H
C
P-Ser CDKs substrate integrated density at G2-phase (a.u) x 10⁵
+/+
–/H
D
Prophases with reduced poleward movement of centrosomes (%)
+/+
–/H
E
Eg5 intensity at centrosome (a.ux10⁴)
+/+
–/H
F
Cells with abnormal spindle geometry (%)
+/+
–/H
G
+/+
–/H
Cyclin A2
EV
1-301
EV
Cyclin A2
1-301
Mre11
Rad50
HA
Cyclin A2
Cyclin A2
1-301
Actin
H
EV
Cyclin A21-301
% Cells with >2 53BP1/γ-H2AX foci
+/+
–/H
I
Prophases with reduced poleward movement of centrosomes (%)
*
+/+
–/H
J
Eg5 intensity at centrosomes (a.u.x10⁴)
*
+/+
–/H
K
Cells with abnormal spindle geometry (%)
*
+/+
–/H

Fig. S16. Distinct cyclin A2 functional domains correct defects in Eg5 centrosome loading and *Mre11* mRNA translation in *Ccna2*$^{-/H}$ MEFs. A, Western blot of indicated proteins in *Ccna2*$^{+/+}$ and *Ccna2*$^{-/H}$ MEFs infected with lentivirus from empty TSIN vector or TSIN containing HA-tagged cyclin A2$^{302-432}$. **B**, Quantification of p-Ser Cdk substrates immunofluorescence in S phase. **C**, Quantification of p-Ser Cdk substrates immunofluorescence in G2 phase. **D**, Incidence of prophases with delayed centrosome movement. **E**, Quantification of Eg5 signals at centrosomes in prophase. **F**, Percentage of metaphase cells with abnormal spindle geometry. **G**, Western blot of *Ccna2*$^{+/+}$ and *Ccna2*$^{-/H}$ MEF lysates infected with control or HA-tagged cyclin A2$^{1-301}$ lentiviruses. **H**, Quantification of cells with >2 γH2AX and 53BP1 co-localized foci in *Ccna2*$^{+/+}$ and *Ccna2*$^{-/H}$ MEFs infected with control or HA-tagged cyclin A2$^{1-301}$ lentiviruses. **I**, Incidence of prophases with reduced centrosome movement. **J**, Quantification of Eg5 signal at centrosomes in prophase. **K**, Percentage of metaphase cells with abnormal spindle geometry. Error bars represent SEM. $N = 3$ independent MEF lines per genotype.

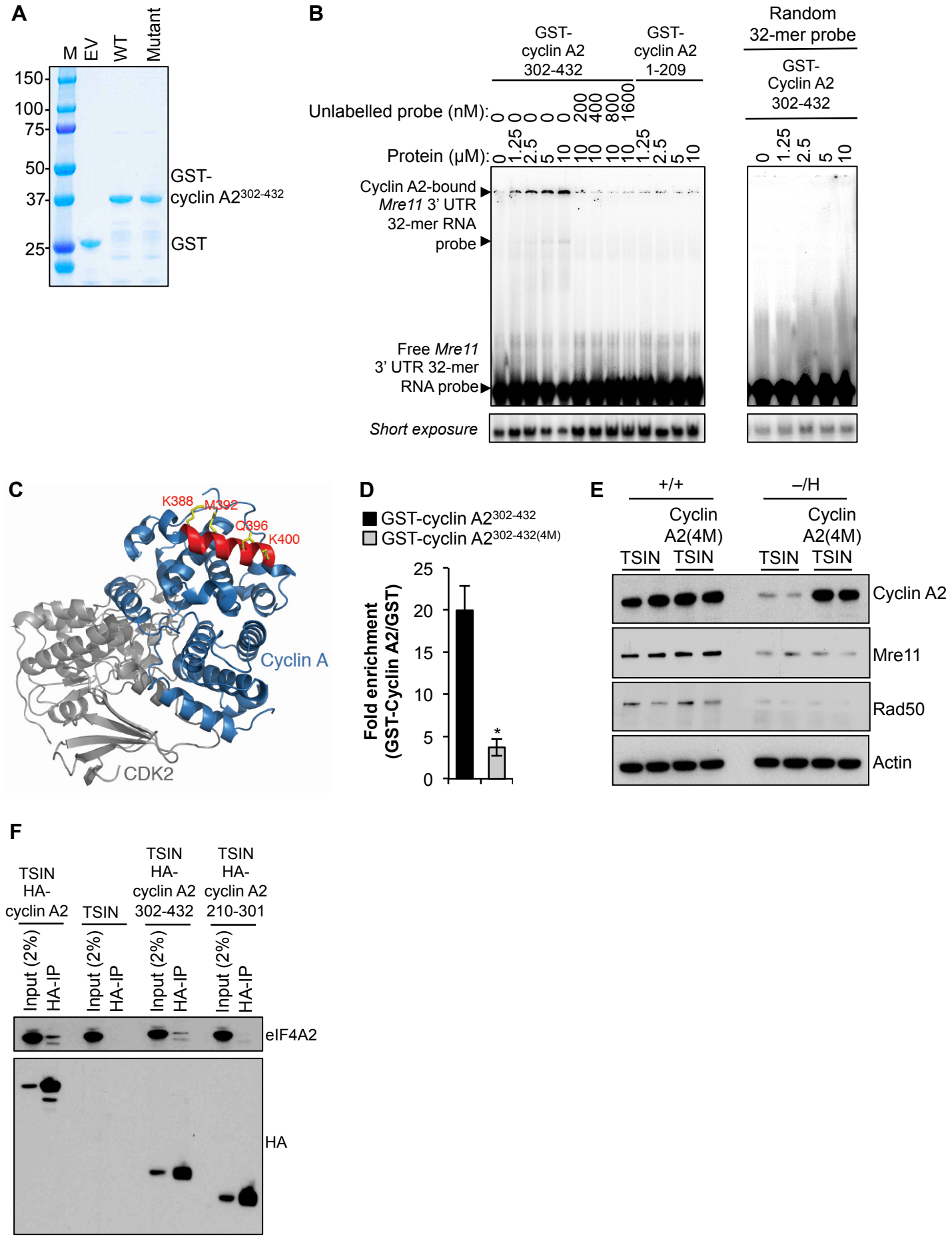
A
M
EV
WT
Mutant
150
100
75
50
37
25
GST-cyclin A2302-432
GST
B
GST-cyclin A2 302-432
GST-cyclin A2 1-209
Random 32-mer probe
GST-Cyclin A2 302-432
Unlabelled probe (nM): 0 0 0 0 200 400 800 1600
Protein (μM): 0 1.25 2.5 5 10 10 10 10 1.25 2.5 5 10
0 1.25 2.5 5 10
Cyclin A2-bound Mre11 3' UTR 32-mer RNA probe
Free Mre11 3' UTR 32-mer RNA probe
Short exposure
C
K388
M392
Q396
K400
Cyclin A
CDK2
D
GST-cyclin A2302-432
GST-cyclin A2302-432(4M)
Fold enrichment (GST-Cyclin A2/GST)
25
20
15
10
5
0
*
E
+/+
–/H
Cyclin A2(4M)
TSIN
Cyclin A2
Mre11
Rad50
Actin
F
TSIN HA-cyclin A2
TSIN
TSIN HA-cyclin A2 302-432
TSIN HA-cyclin A2 210-301
Input (2%)
HA-IP
eIF4A2
HA

Fig. S17. The cyclin A2 C-terminus interacts with the Mre11 3'UTR and eIF4A2. A, Coomassie stained SDS-PAGE gel showing GST (empty vector), GST-cyclin $A2^{302-432}$, and mutant GST-cyclin $A2^{302-432}$ recombinant proteins purified from E. coli. **B**, Native gel shifts demonstrating that cold (unlabeled) Mre11 3' UTR probe eliminates radiolabelled probe from the gel slots, indicating the presence of radiolabelled probe in gel slots represents probe specifically bound to GST-cyclin $A2^{302-432}$ recombinant protein. **C**, Crystal structure of the complex of human cyclin A2 and CDK2 (PDB accession code: 1FIN). On the basis of the three-dimensional structure of cyclin A2, after excluding the binding interface with CDK2, the α-helical region of cyclin A2 encompassing residues 388 to 400 is a good candidate for an RNA interaction motif owing to the positive and polar nature of its solvent-accessible surface. Residues forming the accessible surface (Lys388, Met392, Gln396 and Lys400) where replaced by alanines to eliminate the positive charge and polarity while not disturbing the protein fold by preserving the α-helical conformation. The putative RNA binding α-helix of cyclin A2 is colored red. The solvent-accessible side chains are shown as yellow sticks. **D**, RNA immunoprecipitation with cyclin A2 antibody in an *in vitro* reaction containing purified recombinant wild-type GST-cyclin $A2^{302-432}$ or mutant GST-cyclin $A2^{302-432}$ and *in vitro* transcribed Mre11 3'UTR (1-754 bp). Error bars represent SEM. $N = 3$ independent MEF lines per genotype. Statistical significance was determined by an unpaired *t*-test. $^*P < 0.05$. **E**, Immunoblot analysis of asynchronously cultured MEFs transduced with control (TSIN) or *Ccna2*-containing (cyclin A2(4M)-TSIN) lentiviruses. **F**, Analysis of complex formation between cyclin A2 and eIF4A2 in 293T cells transfected with various HA-tagged domains of cyclin A2 using co-immunoprecipitation assay. Immunoprecipitation was performed with an HA antibody.

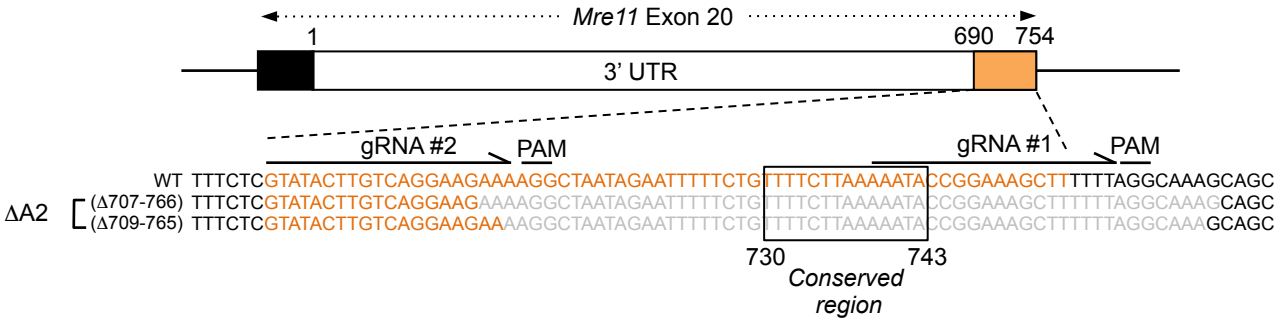

Fig. S18. CRISPR/Cas9-mediated deletion of the 3' end of the *Mre11* 3'UTR in mice. Schematic diagram of the *Mre11* 3'UTR deletion mutant alleles. The structure of *Mre11* exon 20 is shown. The area targeted for deletion is highlighted in orange. Target locations of sgRNAs and corresponding PAM sites used to generate deletion mutants are indicated. Grey font indicates the deleted sequences found in the two founder animals used for the generation of homozygous ΔA2 mice and MEFs.

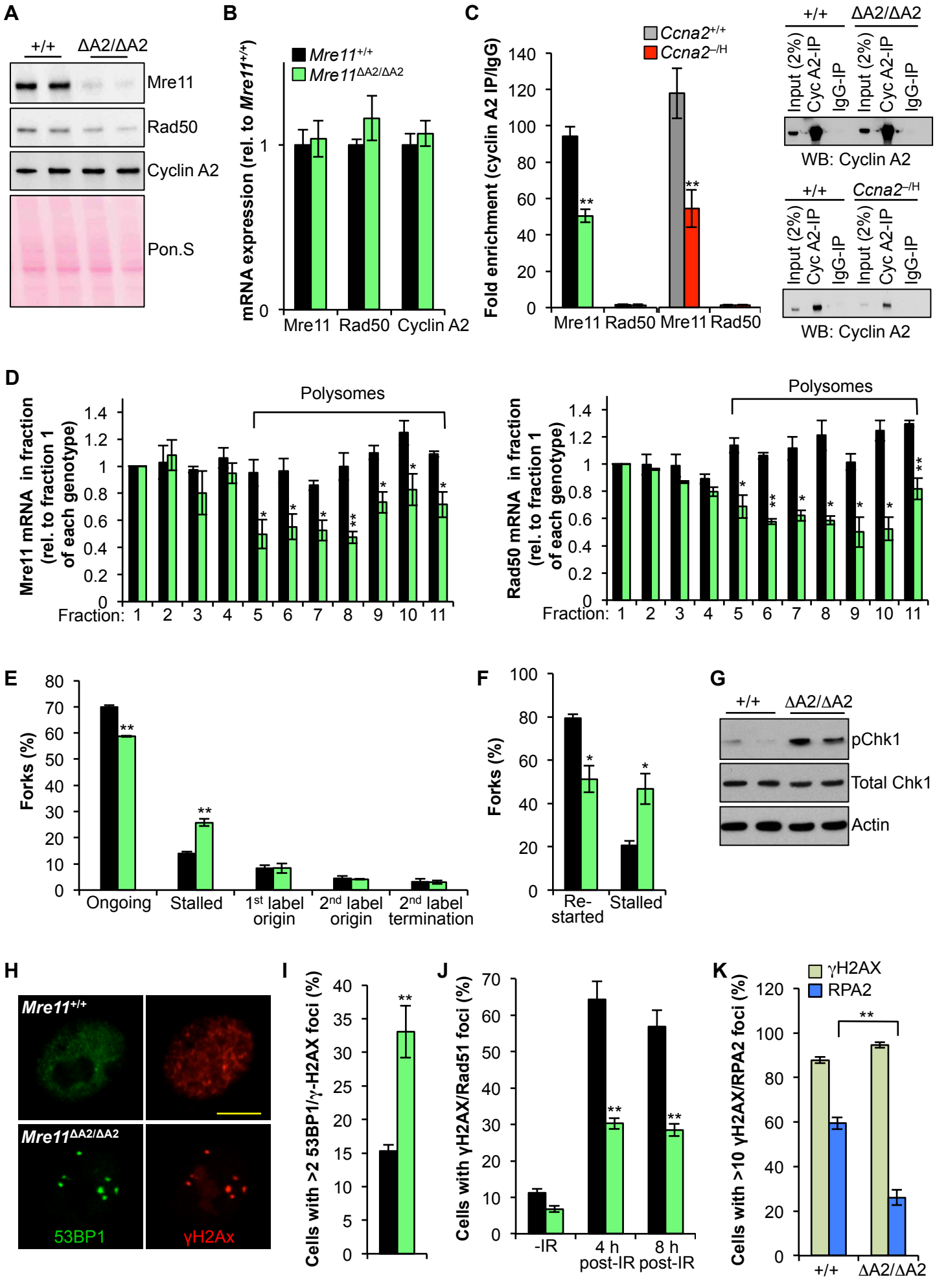
A
+/+
ΔA2/ΔA2
Mre11
Rad50
Cyclin A2
Pon.S
B
mRNA expression (rel. to Mre11+/+)
Mre11+/+
Mre11ΔA2/ΔA2
Mre11 Rad50 Cyclin A2
C
Fold enrichment (cyclin A2 IP/IgG)
Ccna2+/+
Ccna2–/H
Mre11 Rad50 Mre11 Rad50
+/+
ΔA2/ΔA2
Input (2%)
Cyc A2-IP
IgG-IP
WB: Cyclin A2
Ccna2–/H
D
Polysomes
Mre11 mRNA in fraction (rel. to fraction 1 of each genotype)
Rad50 mRNA in fraction (rel. to fraction 1 of each genotype)
Fraction: 1 2 3 4 5 6 7 8 9 10 11
E
Forks (%)
Ongoing
Stalled
1st label origin
2nd label origin
2nd label termination
F
Forks (%)
Re-started
Stalled
G
+/+
ΔA2/ΔA2
pChk1
Total Chk1
Actin
H
Mre11+/+
Mre11ΔA2/ΔA2
53BP1
γH2Ax
I
Cells with >2 53BP1/γ-H2AX foci (%)
J
Cells with γH2AX/Rad51 foci (%)
-IR
4 h post-IR
8 h post-IR
K
γH2AX
RPA2
Cells with >10 γH2AX/RPA2 foci (%)
+/+
ΔA2/ΔA2

Fig. S19. *Mre11*$^{\Delta A2/\Delta A2}$ MEFs mimic the Cdk2-independent phenotypes of *Ccna2*$^{-/H}$ MEFs. A, Immunoblot analysis of indicated proteins in lysates of asynchronous *Mre11*$^{+/+}$ and *Mre11*$^{\Delta A2/\Delta A2}$ MEFs. Mre11 protein levels are reduced when the 3' end of the Mre11 3'UTR is lacking. As for *Ccna2*$^{-/H}$ MEFs, Rad50 expression is dependent on Mre11. As expected, cyclin A2 levels were unperturbed in *Mre11*$^{\Delta A2/\Delta A2}$ MEFs. **B**, Quantitative real-time PCR analysis of indicated mRNAs in *Mre11*$^{+/+}$ and *Mre11*$^{\Delta A2/\Delta A2}$ MEFs. These data indicate the decreased expression of Mre11 and Rad50 in *Mre11*$^{\Delta A2/\Delta A2}$ MEFs is not due to a deficiency in the amount of transcript synthesized. **C**, Quantitation of Mre11 and Rad50 transcripts immunoprecipitated with cyclin A2 antibody in normal *Ccna2*$^{-/H}$ and *Mre11*$^{\Delta A2/\Delta A2}$ MEFs, indicating that lowering cyclin A2 or deleting part of the Mre11 3'UTR results in similar decreases in cyclin A2-bound Mre11 transcripts. **D**, Quantification of polysome-associated *Mre11* mRNA in *Mre11*$^{+/+}$ and *Mre11*$^{\Delta A2/\Delta A2}$ MEFs. Impaired cyclin A2 binding to *Mre11*$^{\Delta A2}$ RNA markedly decreases polysome association, which is consistent with reduced Mre11 protein levels expressed *Mre11*$^{\Delta A2/\Delta A2}$ MEFs. **E**, Analysis of DNA replication in *Mre11*$^{+/+}$ and *Mre11*$^{\Delta A2/\Delta A2}$ MEFs by DNA fiber assay. Consistent with decreased Mre11 expression, replication fork stalling was significantly increased in *Mre11*$^{\Delta A2/\Delta A2}$ MEFs. **F**, Quantification of restarted replication forks after release from HU exposure in *Mre11*$^{+/+}$ and *Mre11*$^{\Delta A2/\Delta A2}$ MEFs showing that, consistent with reduced Mre11 protein expression, the efficiency of replication forks restart is markedly reduced in *Mre11*$^{\Delta A2/\Delta A2}$ MEFs. **G**, Immunoblot analysis of Chk1 S345 phosphorylationin *Mre11*$^{+/+}$ and *Mre11*$^{\Delta A2/\Delta A2}$ MEFs providing evidence for replication stress. Actin was used as a loading control. **H**, Images of *Mre11*$^{+/+}$ and *Mre11*$^{\Delta A2/\Delta A2}$ MEFs immunostained for γH2AX and 53BP1 co-localized foci, demonstrating that reduced Mre11 expression correlates with increased rates of DSBs. **I,** Quantification of cells with >2 γH2AX-53BP1 double-positive foci in the indicated MEFs. **J**, Quantification of cells with >10 γH2AX and Rad51 co-localized foci. **K**, Quantification of cells with >10 γH2AX and RPA2 co-localized foci at 4 h after 10 Gy γ-irradiation. Error bars represent SEM. $N = 3$ independent MEF lines per genotype for all analysis. Statistical significance was determined by an unpaired *t*-test. *$P < 0.05$, **$P < 0.01$.

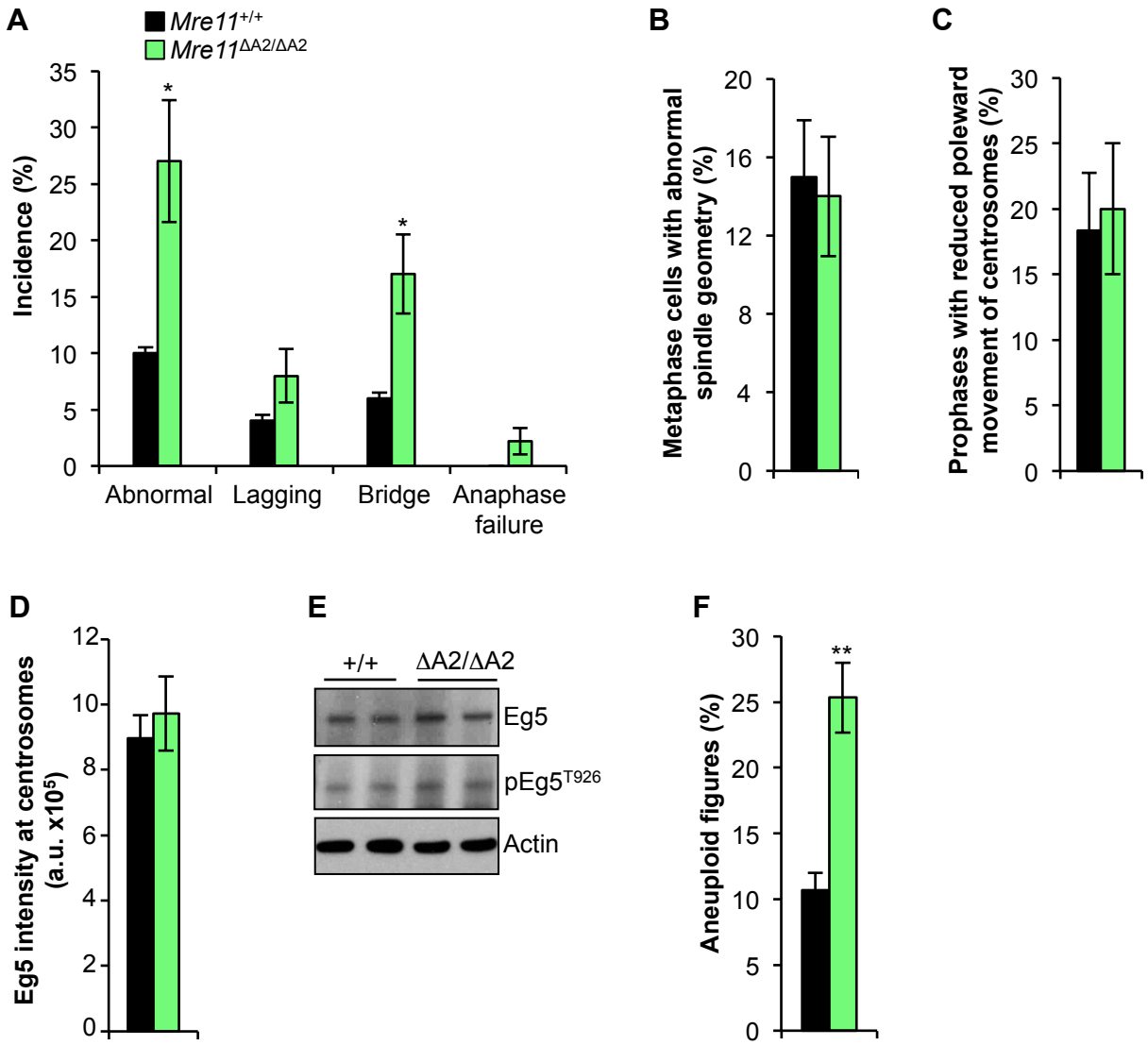

Fig. S20. *Mre11*$^{\Delta A2/\Delta A2}$ MEFs have increased rates of chromatin bridges and aneuploidy. A, Live-cell imaging analysis of chromosome missegregations in H2B-mRFP expressing MEFs. $N = 3$ independent MEF lines per genotype. Chromatin bridges, not lagging chromosomes, are significantly increased. **B-D**, Quantification of metaphases cells with abnormal spindle geometry (**B**), prophases with reduced poleward movement of centrosomes (**C**), and centrosome-associated Eg5 levels prophase cells (**D**). Unlike *Ccna2*$^{-/H}$ MEFs, *Mre11*$^{\Delta A2/\Delta A2}$ MEFs loading of Eg5 onto chromosomes is not impaired, which is consistent normal centrosome dynamics, formation of symmetrical spindles, proper microtubule-kinetochore attachment and normal rates of lagging chromosomes. **E**, Western blot analysis of MEFs lysates for Eg5 expression and phosphorylation. Unlike *Ccna2*$^{-/H}$ MEFs, *Mre11*$^{\Delta A2/\Delta A2}$ MEFs do not show impaired Cdk2-mediated phosphorylation of Eg5 at T926, which is consistent with normal Eg5 loading onto chromosomes. **F**, Karyotype analysis of P5 MEFs showing that increased chromatin bridging in *Mre11*$^{\Delta A2/\Delta A2}$ MEFs corresponds to increased aneuploidization. Error bars represent SEM. $N = 3$ independent MEF lines per genotype. Statistical significance was determined by an unpaired *t*-test. *$P < 0.05$, **$P < 0.01$.

Captions for Tables S1 to S3

Table S1. Cyclin A2 RIP-seq data (separate xls.file)

Table S2. Cyclin E1 RIP-seq data (separate xls.file)

Table S3. Cyclin B1 RIP-seq data (separate xls.file)

Table S4 Primers used for the generation and genotyping of *Mre11*$^{\Delta A2}$ mutant mice

Primer	**Sequence (5'-3')**
sgRNA generation	
gRNA 1 FWD	CACCGAAATACCGGAAAGCTTTTTT
gRNA 1 Complement	aaacAAAAAAGCTTTCCGGTATTTC
gRNA-1 T7 Fwd	ttaatacgactcactatagGAAATACCGGAAAGCTTTTTT
gRNA2 fwd	CACCGTATACTTGTCAGGAAGAAA
gRNA 2 complement	AAACTTTCTTCCTGACAAGTATAC
gRNA-2 T7 Fwd	ttaatacgactcactatagGGTATACTTGTCAGGAAGAAA
T7-sgRNA_R	AAAAGCACCGACTCGGTGCC
Genotyping primes	
Mre11 3UTR Del FW	CCTCTGTGCCACAGCTAGCAGTTG
Mre11 3UTR Del Rev	GCAGAAGTTTTTAGAGTGTGGGACAGGG

References

1. H. Hochegger, S. Takeda, T. Hunt, Cyclin-dependent kinases and cell-cycle transitions: Does one fit all? *Nat. Rev. Mol. Cell Biol.* **9**, 910–916 (2008). Medline doi:10.1038/nrm2510

2. H. Beamish, L. de Boer, N. Giles, F. Stevens, V. Oakes, B. Gabrielli, Cyclin A/cdk2 regulates adenomatous polyposis coli-dependent mitotic spindle anchoring. *J. Biol. Chem.* **284**, 29015–29023 (2009). Medline doi:10.1074/jbc.M109.042820

3. L. Kabeche, D. A. Compton, Cyclin A regulates kinetochore microtubules to promote faithful chromosome segregation. *Nature* **502**, 110–113 (2013). Medline doi:10.1038/nature12507

4. N. Arsic, N. Bendris, M. Peter, C. Begon-Pescia, C. Rebouissou, G. Gadéa, N. Bouquier, F. Bibeau, B. Lemmers, J. M. Blanchard, A novel function for Cyclin A2: Control of cell invasion via RhoA signaling. *J. Cell Biol.* **196**, 147–162 (2012). Medline doi:10.1083/jcb.201102085

5. M. Murphy, M. G. Stinnakre, C. Senamaud-Beaufort, N. J. Winston, C. Sweeney, M. Kubelka, M. Carrington, C. Bréchot, J. Sobczak-Thépot, Delayed early embryonic lethality following disruption of the murine cyclin A2 gene. *Nat. Genet.* **15**, 83–86 (1997). Medline doi:10.1038/ng0197-83

6. I. Kalaszczynska, Y. Geng, T. Iino, S. Mizuno, Y. Choi, I. Kondratiuk, D. P. Silver, D. J. Wolgemuth, K. Akashi, P. Sicinski, Cyclin A is redundant in fibroblasts but essential in hematopoietic and embryonic stem cells. *Cell* **138**, 352–365 (2009). Medline doi:10.1016/j.cell.2009.04.062

7. C. H. Yam, T. K. Fung, R. Y. Poon, Cyclin A in cell cycle control and cancer. *Cell. Mol. Life Sci.* **59**, 1317–1326 (2002). Medline doi:10.1007/s00018-002-8510-y

8. M. Serrano, H. Lee, L. Chin, C. Cordon-Cardo, D. Beach, R. A. DePinho, Role of the INK4a locus in tumor suppression and cell mortality. *Cell* **85**, 27–37 (1996). Medline doi:10.1016/S0092-8674(00)81079-X

9. R. M. Naylor, K. B. Jeganathan, X. Cao, J. M. van Deursen, Nuclear pore protein NUP88 activates anaphase-promoting complex to promote aneuploidy. *J. Clin. Invest.* **126**, 543–559 (2016). Medline doi:10.1172/JCI82277

10. J. H. van Ree, H. J. Nam, K. B. Jeganathan, A. Kanakkanthara, J. M. van Deursen, Pten regulates spindle pole movement through Dlg1-mediated recruitment of Eg5 to centrosomes. *Nat. Cell Biol.* **18**, 814–821 (2016). Medline

11. A. Slangy, H. A. Lane, P. d'Hérin, M. Harper, M. Kress, E. A. Niggt, Phosphorylation by p34cdc2 regulates spindle association of human Eg5, a kinesin-related motor essential for bipolar spindle formation in vivo. *Cell* **83**, 1159–1169 (1995). Medline doi:10.1016/0092-8674(95)90142-6

12. H. J. Nam, J. M. van Deursen, Cyclin B2 and p53 control proper timing of centrosome separation. *Nat. Cell Biol.* **16**, 538–549 (2014). Medline doi:10.1038/ncb2952

13. R. A. Burrell, S. E. McClelland, D. Endesfelder, P. Groth, M. C. Weller, N. Shaikh, E. Domingo, N. Kanu, S. M. Dewhurst, E. Gronroos, S. K. Chew, A. J. Rowan, A. Schenk, M. Sheffer, M. Howell, M. Kschischo, A. Behrens, T. Helleday, J. Bartek, I. P. Tomlinson, C. Swanton, Replication stress links structural and numerical cancer chromosomal instability. *Nature* **494**, 492–496 (2013). Medline doi:10.1038/nature11935

14. M. K. Zeman, K. A. Cimprich, Causes and consequences of replication stress. *Nat. Cell Biol.* **16**, 2–9 (2014). Medline doi:10.1038/ncb2897

15. T. H. Stracker, J. H. Petrini, The MRE11 complex: Starting from the ends. *Nat. Rev. Mol. Cell Biol.* **12**, 90–103 (2011). Medline doi:10.1038/nrm3047

16. F. W. Pagliuca, M. O. Collins, A. Lichawska, P. Zegerman, J. S. Choudhary, J. Pines, Quantitative proteomics reveals the basis for the biochemical specificity of the cell-cycle machinery. *Mol. Cell* **43**, 406–417 (2011). Medline doi:10.1016/j.molcel.2011.05.031

17. M. M. Dawlaty, J. M. van Deursen, Gene targeting methods for studying nuclear transport factors in mice. *Methods* **39**, 370–378 (2006). Medline doi:10.1016/j.ymeth.2006.06.009

18. J. R. Babu, K. B. Jeganathan, D. J. Baker, X. Wu, N. Kang-Decker, J. M. van Deursen, Rae1 is an essential mitotic checkpoint regulator that cooperates with Bub3 to prevent chromosome missegregation. *J. Cell Biol.* **160**, 341–353 (2003). Medline doi:10.1083/jcb.200211048

19. A. Hodgkins, A. Farne, S. Perera, T. Grego, D. J. Parry-Smith, W. C. Skarnes, V. Iyer, WGE: A CRISPR database for genome engineering. *Bioinformatics* **31**, 3078–3080 (2015). Medline doi:10.1093/bioinformatics/btv308

20. H. Yang, H. Wang, R. Jaenisch, Generating genetically modified mice using CRISPR/Cas-mediated genome engineering. *Nat. Protoc.* **9**, 1956–1968 (2014). Medline doi:10.1038/nprot.2014.134

21. L. Cong, F. A. Ran, D. Cox, S. Lin, R. Barretto, N. Habib, P. D. Hsu, X. Wu, W. Jiang, L. A. Marraffini, F. Zhang, Multiplex genome engineering using CRISPR/Cas systems. *Science* **339**, 819–823 (2013). Medline doi:10.1126/science.1231143

22. K. B. Jeganathan, L. Malureanu, J. M. van Deursen, The Rae1-Nup98 complex prevents aneuploidy by inhibiting securin degradation. *Nature* **438**, 1036–1039 (2005). Medline doi:10.1038/nature04221

23. J. H. van Ree, K. B. Jeganathan, L. Malureanu, J. M. van Deursen, Overexpression of the E2 ubiquitin-conjugating enzyme UbcH10 causes chromosome missegregation and tumor formation. *J. Cell Biol.* **188**, 83–100 (2010). Medline doi:10.1083/jcb.200906147

24. T. Miest, D. Saenz, A. Meehan, M. Llano, E. M. Poeschla, Intensive RNAi with lentiviral vectors in mammalian cells. *Methods* **47**, 298–303 (2009). Medline doi:10.1016/j.ymeth.2008.11.001

25. K. Jeganathan, L. Malureanu, D. J. Baker, S. C. Abraham, J. M. van Deursen, Bub1 mediates cell death in response to chromosome missegregation and acts to suppress spontaneous tumorigenesis. *J. Cell Biol.* **179**, 255–267 (2007). Medline doi:10.1083/jcb.200706015

26. M. M. Dawlaty, L. Malureanu, K. B. Jeganathan, E. Kao, C. Sustmann, S. Tahk, K. Shuai, R. Grosschedl, J. M. van Deursen, Resolution of sister centromeres requires RanBP2-mediated SUMOylation of topoisomerase IIα. *Cell* **133**, 103–115 (2008). Medline doi:10.1016/j.cell.2008.01.045

27. S. T. Eblen, M. P. Fautsch, R. A. Anders, E. B. Leof, Conditional binding to and cell cycle-regulated inhibition of cyclin-dependent kinase complexes by p27Kip1. *Cell Growth Differ.* **6**, 915–925 (1995). Medline

28. R. M. Ricke, K. B. Jeganathan, L. Malureanu, A. M. Harrison, J. M. van Deursen, Bub1 kinase activity drives error correction and mitotic checkpoint control but not tumor suppression. *J. Cell Biol.* **199**, 931–949 (2012). Medline doi:10.1083/jcb.201205115

29. D. J. Baker, B. G. Childs, M. Durik, M. E. Wijers, C. J. Sieben, J. Zhong, R. A. Saltness, K. B. Jeganathan, G. C. Verzosa, A. Pezeshki, K. Khazaie, J. D. Miller, J. M. van Deursen, Naturally occurring p16(Ink4a)-positive cells shorten healthy lifespan. *Nature* **530**, 184–189 (2016). Medline doi:10.1038/nature16932

30. T. Peritz, F. Zeng, T. J. Kannanayakal, K. Kilk, E. Eiríksdóttir, U. Langel, J. Eberwine, Immunoprecipitation of mRNA-protein complexes. *Nat. Protoc.* **1**, 577–580 (2006). Medline doi:10.1038/nprot.2006.82

31. K. R. Kalari, A. A. Nair, J. D. Bhavsar, D. R. O'Brien, J. I. Davila, M. A. Bockol, J. Nie, X. Tang, S. Baheti, J. B. Doughty, S. Middha, H. Sicotte, A. E. Thompson, Y. W. Asmann, J. P. Kocher, MAP-RSeq: Mayo Analysis Pipeline for RNA sequencing. *BMC Bioinformatics* **15**, 224 (2014). Medline doi:10.1186/1471-2105-15-224

32. L. Wang, S. Wang, W. Li, RSeQC: Quality control of RNA-seq experiments. *Bioinformatics* **28**, 2184–2185 (2012). Medline doi:10.1093/bioinformatics/bts356

33. C. Trapnell, L. Pachter, S. L. Salzberg, TopHat: Discovering splice junctions with RNA-Seq. *Bioinformatics* **25**, 1105–1111 (2009). Medline doi:10.1093/bioinformatics/btp120

34. B. Langmead, C. Trapnell, M. Pop, S. L. Salzberg, Ultrafast and memory-efficient alignment of short DNA sequences to the human genome. *Genome Biol.* **10**, R25 (2009). Medline doi:10.1186/gb-2009-10-3-r25

35. S. Anders, P. T. Pyl, W. Huber, HTSeq—a Python framework to work with high-throughput sequencing data. *Bioinformatics* **31**, 166–169 (2015). Medline doi:10.1093/bioinformatics/btu638

36. M. D. Robinson, D. J. McCarthy, G. K. Smyth, edgeR: A Bioconductor package for differential expression analysis of digital gene expression data. *Bioinformatics* **26**, 139–140 (2010). Medline doi:10.1093/bioinformatics/btp616

37. V. R. Gerbasi, C. M. Weaver, S. Hill, D. B. Friedman, A. J. Link, Yeast Asc1p and mammalian RACK1 are functionally orthologous core 40S ribosomal proteins that repress gene expression. *Mol. Cell. Biol.* **24**, 8276–8287 (2004). Medline doi:10.1128/MCB.24.18.8276-8287.2004

38. J. Buis, T. Stoneham, E. Spehalski, D. O. Ferguson, Mre11 regulates CtIP-dependent double-strand break repair by interaction with CDK2. *Nat. Struct. Mol. Biol.* **19**, 246–252 (2012). Medline doi:10.1038/nsmb.2212